Halogens in proto-Iceland plume basalts

Emma L. Tomlinson[1*], Estelle F. Rose-Koga[2], Anne-Sophie Bouvier[3], Donal O'Farrell[1], John T. Caulfield[4], Matthew G. Jackson[5], Yves Moussallam[6], Finlay M. Stuart[7] and Johan Villeneuve[8].

[1]Geology, School of Natural Sciences, Trinity College Dublin, Dublin, Ireland.
[2]Earth Sciences Institute of Orléans, University Orléans, CNRS, Orléans, France.
[3]Institut des Sciences de la Terre, University of Lausanne, Lausanne, Switzerland.
[4]School of Earth and Atmospheric Sciences, Queensland University of Technology, Brisbane, Queensland, Australia.
[5]Department of Earth Science, University of California Santa Barbara, Santa Barbara, California, USA.
[6]Department of Earth and Environmental Sciences, Columbia University, New York, USA.
[7]Scottish Universities Environmental Research Centre, East Kilbride, South Lanarkshire, UK.
[8]Centre de Recherches Pétrographiques et Géochimiques, CNRS, Université de Lorraine, Vandœuvre-lès-Nancy, France.
*corresponding author

Abstract

Melt inclusions in olivine phenocrysts from high $^{3}He/^{4}He$ proto-Iceland plume (PIP) basalts from Baffin Island and West Greenland have elevated Br/Cl ratios, extending to values significantly above those found in mid ocean ridge (MORB) and ocean island basalts (OIB). Chlorine isotope compositions are indistinguishable from MORB-source mantle and high Br/Cl occurs in the absence of geochemical indicators for serpentinite, altered oceanic crust or sediment. The highest Br/Cl occur in melt inclusions from basalts with the highest $^{3}He/^{4}He$. The high Br/Cl ratios are at the high end of the range of putative Earth-source meteorites (CI- and CM-type carbonaceous chondrites). The PIP melt inclusion compositions are consistent with the addition of a small volume of halogen-rich, high Br/Cl chondritic material to halogen-depleted, low Br/Cl mantle.

Introduction

The halogens (F, Cl, Br, I) have proved to be valuable tracers of recycled marine sediment, altered oceanic crust and serpentinite in the Earth's mantle (Kendrick *et al.*, 2017). This recycled crustal material tends to dominate the halogen inventory of the convecting mantle (Kendrick *et al.*, 2017) likely masking the primordial halogen inventory. The relative abundances of Cl and Br in geochemically enriched intra-plate basalt glasses from Hawaii, Samoa, Society and Pitcairn are essentially indistinguishable from mid-ocean ridge basalts, implying that the convecting mantle is homogenous in terms of halogens (Kendrick *et al.*, 2014; Kendrick *et al.*, 2015; Kendrick *et al.*, 2025). However, the Earth's mantle is depleted in halogens relative to chondritic meteorites. While the depletion of F aligns with its condensation temperature, Cl and Br concentrations are an order of magnitude lower than predicted by the volatility trend (Lodders and Fegley, 1998). One possible explanation for this discrepancy is the presence of a halogen-rich reservoir in the deep Earth. The recent discovery of elevated Br/Cl in melt-inclusion bearing olivine from high $^{3}He/^{4}He$ basalts from Koko and Suiko in the Emperor Seamount (Broadley *et al.*, 2019) chain provides the first indication of halogen heterogeneity in the mantle that may be associated with a deep mantle source.

The picritic flood basalts from Baffin Island (Clarke and Upton, 1971) and West Greenland (Larsen *et al.*, 1992) were erupted at around 61 Ma and are believed to be the earliest volcanic products from the Iceland plume. These proto-Iceland plume (PIP) basalts have the highest mantle-derived $^{3}He/^{4}He$ ratios recorded to date (Stuart *et al.*, 2003; Starkey *et al.*, 2009). The high $^{3}He/^{4}He$ PIP lavas have a large compositional range but tend to be geochemically depleted in terms of trace elements and radiogenic isotope compositions with only a few enriched basalts (Starkey *et al.*, 2009; Willhite *et al.*, 2019). In this contribution we report the F, Cl and Br compositions of melt inclusions in olivine phenocrysts from high $^{3}He/^{4}He$ basalts from Baffin island and West Greenland in an effort to characterise the heavy halogen composition of the ^{3}He-rich deep mantle reservoir.

Geological setting

The PIP basalts are sub-divided into a depleted N-type (La/Sm_N <0.7) and more enriched E-type (Kent *et al.*, 2004). Both basalt types are depleted relative to the majority of OIB with respect to Sr-Nd-Pb isotopes (Starkey *et al.*, 2009; Willhite *et al.*, 2019). Based on incompatible trace elements and Sr-Nd-Pb-Os-O isotopes the N- and E-type magmas are not related by partial melting, fractional crystallisation or by crustal or lithospheric assimilation (Kent *et al.*, 2004). Instead, the compositional differences are attributed to melting of a heterogeneous mantle (Stuart *et al.*, 2003; Kent *et al.*, 2004). Herzberg and O'Hara (2002) calculate that the Baffin Island picrites formed by relatively high degrees of fractional melting of asthenospheric mantle, around 10-11% (depleted source) and 23-25% (enriched source) at 120-70 km depth.

The studied samples are olivine-phyric N- and E-type basalts from Padloping Island and Cape Searle, Baffin Island, and Disko Island and Nuussuaq, West Greenland and were previously studied by Stuart *et al.* (2003) and Starkey *et al.*, (2009, 2012). They are high-Mg (MgO >13 wt%) picritic lavas that were selected because of their high $^{3}He/^{4}He$ (26 to 49.5 R_a) and because their bulk rock compositions are minimally affected by crustal contamination, indicated by high Nb/Th (9-14) and low K/Nb (81-331). We opted to study melt inclusions, rather than whole rock basalts as they are more likely to record pristine volatile compositions. The host olivines are 300-500 μm diameter and have magnesian cores (100Mg/Mg+Fe mol. 86-87), indicating equilibrium with the least fractionated PIP basalt (Starkey *et al.*, 2012).

The elemental and isotopic ($\delta^{37}Cl$) halogen compositions of PIP melt inclusions were analysed by secondary ion mass spectrometry (SIMS), see supplementary information. The dataset is provided in table S-1 and summarised in table 1. Halogen concentrations were calibrated using a suite of natural basalt glasses. The limit of detection (LoD) is calculated using the formula $LoD = 3.33\sigma/S$, where σ is the standard deviation of the intercept and S is the slope of the calibration curve. We report uncertainties as 2σ, where σ is calculated from the standard deviations of the slope and intercept of the calibration curve. Halogen ratios were calculated for individual melt inclusions and sample averages are calculated from these ratios. The Cl and Br concentrations of MPI-DING glass StHs6/80-G are within ±10% of the preferred values and precision for repeat analysis of F, Cl and Br in MPI-DING glass StHs6/80-G was typically ±10%.

Halogen composition of PIP basalt melt inclusions

Average melt inclusion compositions in the PIP samples are F = 174-440 $\mu g.g^{-1}$, Cl = 78-100 $\mu g.g^{-1}$ and Br = 530-1100 $ng.g^{-1}$. Concentrations of Cl and Br are significantly lower than those reported in enriched, EM-type and HIMU (high μ, $\mu = {}^{238}U/{}^{204}Pb$) glasses from Samoa, Society and Pitcairn (Kendrick *et al.*, 2014; Kendrick *et al.*, 2015) and are at the lower end of values reported for depleted OIB from Hawaii (Kendrick *et al.*, 2025) (Fig. 1a,b). Low halogen concentrations have previously been recorded in basaltic glasses from E-type PIP lavas from Baffin Island (Kendrick *et al.*, 2015). The PIP basalts analysed here have K/Cl of 27-62 and $^{87}Sr/^{86}Sr$ of 0.7030-0.7034 that plot at the enriched end of the MORB array (Fig. 1c).

Chlorine isotopes can be used as tracers of recycled chlorine in the mantle (John *et al.*, 2010). The chlorine isotope composition ($\delta^{37}Cl$) of three PIP basalt melt inclusions range from -0.2 to +0.6 ‰ (SMOC). This range overlaps the mantle value (−0.2 ± 0.5 ‰ (1σ); Sharp *et al.*, 2007) (Fig. 1d) and is lower than EM-type basalts which have more positive $\delta^{37}Cl$ (John *et al.*, 2010).

A key observation is that N- and E-type PIP Melt inclusions in samples have 1000Br/Cl ratios (6.7 to 12.4) that are significantly higher than recorded by MORB and OIB (2.8 ± 0.8; Kendrick *et al.*, 2017). These are also higher than Br/Cl ratios recorded in low $^{3}He/^{4}He$ E-type basalts from Baffin Island (Kendrick *et al.*, 2015) (Fig. 2a,b). The highest values are outside of uncertainty of MORB mantle value at 2σ. Importantly the samples with the highest $^{3}He/^{4}He$ have the highest Br/Cl ratios, although any correlation is obscured by the large uncertainty (Fig. 2c).

Contamination

The Br/Cl ratio of basaltic melt can increase during interaction with seawater-derived brines in the crust, either before emplacement within the magma chamber or after emplacement during alteration (Kendrick *et al.*, 2013a). However, only one of the studied basalts was emplaced in a submarine setting, the others being subaerial or hypabyssal (table 1). In addition, the PIP Melt inclusions do not show the low K/Cl and F/Cl ratios and the negative correlations of these ratios with Br/Cl that characterize mixing with saline brine (Kendrick *et al.*, 2013a) (Fig. 2a).

The PIP basalt sequence was erupted through continental lithosphere and high grade crustal basement (Robillard *et al.*, 1992) and the high Br/Cl ratios may have been generated during interaction of the melts with the lithosphere and/or crust during ascent. Peridotite xenoliths from the lithospheric mantle have high Br/Cl ratios, a feature that has been attributed to metasomatism by subduction-related fluids (Broadley *et al.*, 2016). Similarly, while lower continental crust has low halogen concentrations and low Br/Cl, organic matter within upper continental crust has elevated Br/Cl (Han *et al.*, 2023). Assimilation of metasomatised lithosphere or organic-rich upper continental crust could impart high Br/Cl ratios to the basaltic melts. However, the PIP basalts in this study lack the elevated LILE/HREE ratios, HFSE depletions and radiogenic Sr isotope compositions that are indicative of incorporation of altered oceanic crust and lithosphere (Fig. 1c). Furthermore, it is difficult to explain the co-occurrence of high Br/Cl and high $^{3}He/^{4}He$ by reactivation of subducted or crustal halogens. Therefore, we suggest that the high Br/Cl ratios are likely to be characteristic of the high $^{3}He/^{4}He$ PIP source.

Halogen composition of the proto-Iceland plume mantle source region

The composition of the N-type and E-type mantle sources were estimated by accumulated fractional melt modelling assuming modal melting (see supplementary information). We use the composition of melt inclusions in samples PI-25 and CS-6 to represent melts from the depleted and enriched asthenospheric mantle, respectively, and assume melt fractions of 0.1 for the depleted melt and 0.25 for the enriched melt, as appropriate for melting of the PIP source (Herzberg and O'Hara, 2002). We use partition coefficients D_F, and D_{Cl} from Joachim *et al.* (2015) and consider Br and Cl to be similarly incompatible. The calculated halogen composition of the source mantle is shown in figure 3 and table S-6, and the 1000Br/Cl ratio is 9.3 (PI-25) and 6.9 (CS-6).

The halogen compositions of bulk silicate Earth (BSE) and depleted mantle (DM) are estimated from the currently available OIB and MORB data (table S-6). The calculated K, F and Cl contents of the mantle source of the N-type and E-type PIP basalts are broadly within range of most estimates of DM and BSE. However, the calculated Br content of the PIP sources is significantly higher than DM and BSE (Fig. 3), resulting in Br/Cl ratios that are 2-4 times higher than DM and BSE.

Scenario 1: Addition of recycled halogens to the Iceland mantle plume source

Subducted sediments can have elevated Br/Cl ratios of 4.9±1.5 but with individual analyses extending to ~100 (Han *et al.*, 2023). The $\delta^{37}Cl$ composition of subducted sediment ranges from -3.7 to +2.4 ‰ (Barnes and Sharp, 2017) and thus overlaps the mantle-like chlorine isotope composition of the PIP basalt melt inclusions and cannot exclude subducted sediment as the source of the high Br/Cl ratios. However, the PIP basalts are depleted and lack the elevated $^{87}Sr/^{86}Sr$ signatures typically associated with subducted sediment (Fig. 1c, Fig. 2b). Therefore, a recycled sediment origin for the higher Br/Cl ratios is only possible if the halogens are decoupled from lithophile trace elements during sediment devolatilization, however Cl is known to enhance the solubility of trace elements, including Sr, via chloride complexing such that Sr is compatible in saline fluid (e.g. Keppler (2017)). In addition, volcanic glasses that do have radiogenic $^{87}Sr/^{86}Sr$ compositions associated with the presence of recycled sediment do not have elevated Br/Cl contents (Kendrick *et al.*, 2017).

Br/Cl ratios like those in the PIP melt inclusions are found in sedimentary marine pore fluids and in serpentinite (Kendrick *et al.*, 2013b) (Fig. 2). Sedimentary pore fluids extend from mantle-like compositions to strongly negative $\delta^{37}Cl$ values of -8 ‰, with most of the available data sitting to the negative side of the terrestrial value (Barnes and Sharp, 2017), this means that sedimentary pore fluids are a possible, but less likely source of high Br/Cl in the PIP melt inclusions. Serpentinite is a more plausible candidate because the $\delta^{37}Cl$ averages -0.1‰. Broadley *et al.* (2019) report high Br/Cl in crushed olivine from high $^{3}He/^{4}He$ basalts from Suiko and Koko in the Emperor seamounts chain, where the halogens were inferred to reside in fluid and/or melt inclusions, they attribute high Br/Cl to incorporation of altered oceanic crust and dehydrated serpentinite into the high $^{3}He/^{4}He$ Hawaii plume source. However, serpentinites are characterised by strongly radiogenic $^{87}Sr/^{86}Sr$ compositions and low K/Cl that are not seen in the PIP basalts (Fig. 1c). Furthermore, the PIP basalts lack elevated Fe/Mn and depleted Ca associated with the presence of eclogite or pyroxenite and have primitive Nd isotope compositions, consistent with an absence of recycled oceanic crust (Jackson *et al.*, 2010). Therefore, while serpentinite may be the source of the high Br/Cl ratios in the PIP melt inclusions, its contribution to the lithophile element inventory was minimal. .

Scenario 2: High Br/Cl mantle

An alternative interpretation is that elevated Br/Cl ratios are intrinsic to the deep mantle. In this scenario, the low halogen content of the convecting mantle is due to depletion during crust formation, while the lower Br/Cl is due to incorporation of low Br/Cl recycled material. One option is that the deep mantle source of the PIP lavas is a heavy halogen-poor, high Br/Cl lower mantle reservoir. Such a source must be heterogeneous to account for the presence of both N- and E-type PIP basalts both with high $^{3}He/^{4}He$ and high Br/Cl. Therefore, the PIP melts may be more easily explained by addition of a small volume of heavy halogen-rich, high Br/Cl deep mantle to halogen-poor mantle.

Current estimates for BSE suggest that the mantle is depleted in Cl and Br relative to chondritic meteorites. In addition, although Cl and Br have similar condensation temperatures, the limited available data suggest that chondritic meteorites have higher Br/Cl ratios than BSE, with most estimates being close to the average solar system value of 4.7 (Lodders and Fegley, 1998). The Br/Cl ratio of the PIP melt inclusions is within range but at the upper end of compositions reported for CI- and CM-type carbonaceous chondrites (Fig. 3b), the subtypes of carbonaceous chondrites that most closely resemble the source of volatile elements delivered to the Earth (Alexander *et al.*, 2012). Together, this implies that the primordial mantle may have been more halogen-rich had higher Br/Cl ratios than the convecting mantle, and so incorporation of a small vestige of primitive mantle material into depleted/enriched mantle at the core mantle boundary could explain the unusual halogen composition of the PIP melts. Alternatively, the halogen-rich, high Br/Cl PIP source may reflect a deep mantle heterogeneity, perhaps related to the Earth's accretion and degassing history.

Scenario 3: Addition of heavy halogens from the core

The low chlorine content of BSE may be reconciled with the composition of chondritic meteorites if the core is a significant reservoir for the heavy halogens (Yuan and Steinle-Neumann, 2024). Halogens may reside in the core if they partitioned into liquid metal during core formation. High-pressure experiments indicate that Cl shows lithophile to mildly compatible behaviour (Yuan and Steinle-Neumann, 2024). Bromine partitioning behaviour at high pressure is unknown, however if halogens become more compatible in metal with increasing atomic number, then the core could potentially have a high Br/Cl ratio. However, if Br is mildly compatible in the core, it would be difficult to explain why Br would be transferred out of the core into PIP source.

Conclusions and implications

Melt inclusions in olivine from high $^{3}He/^{4}He$ PIP basalts are halogen-poor and have high Br/Cl ratios relative to MORB and the majority of OIB. The absence of elemental and radiogenic isotope evidence for recycled crustal material in the PIP basalt source, and the absence of elevated Br/Cl in OIB where recycled material is thought to be present, suggest that recycled halogens may not be the source of the elevated Br/Cl ratios in the PIP melt inclusions.

The high Br/Cl ratios are within range of those of chondritic meteorites that may have delivered volatiles to the early Earth. The PIP melt inclusion compositions are consistent with

the addition of a small vestige of halogen-rich, high Br/Cl chondritic material to halogen-poor, low Br/Cl mantle. The presence of a halogen-rich, high Br/Cl chondritic reservoir in deep Earth could explain the apparent deficit of heavy halogens in the Earth relative to chondritic meteorites. Alternatively, the halogen-rich, high Br/Cl mantle source may reflect heterogeneity related to the Earth's accretion history.

The occurrence of these high Br/Cl melts has implications for our understanding of the cycling and homogenisation of halogens in the mantle, as well as the halogen composition and degassing history of the Earth. The high Br/Cl component may be easier to detect in depleted OIB magmas, where the signature is less strongly overprinted by recycled halogens.

Acknowledgements

The authors thank the handling editor Romain Tartèse and Mark Kendrick and Ray Burgess for constructive and thoughtful reviews. This research was funded by SFI grant 15/ERC/B3131 'Halogen' to ELT. The iCRAG laboratory was supported by SFI/RI/3227. ER-K acknowledges SYSTER-INSU-CNRS "Halogens history". Professor J. Godfrey Fitton is thanked for supplying samples collected in 1996 by Ian Snape, Coleen Cole and Sally Brown during an Edinburgh University expedition to Baffin Island supported by the Laidlaw-Hall Trust.

References

Alexander, C.M.O.D., Bowden, R., Fogel, M.L., Howard, K.T., Herd, C.D.K., Nittler, L.R. (2012) The Provenances of Asteroids, and Their Contributions to the Volatile Inventories of the Terrestrial Planets. *Science* 337, 721-723.

Barnes, J.D., Sharp, Z.D. (2017) Chlorine Isotope Geochemistry. *Reviews in Mineralogy and Geochemistry* 82.

Broadley, M.W., Ballentine, C.J., Chavrit, D., Dallai, L., Burgess, R. (2016) Sedimentary halogens and noble gases within Western Antarctic xenoliths: Implications of extensive volatile recycling to the sub continental lithospheric mantle. *Geochimica Et Cosmochimica Acta* 176, 139-156.

Broadley, M.W., Sumino, H., Graham, D.W., Burgess, R., Ballentine, C.J. (2019) Recycled components in mantle plumes deduced from variations in halogens (Cl, Br, and I), trace elements, and He-3/He-4 along the Hawaiian-Emperor seamount chain. *Geochemistry Geophysics Geosystems* 20, 277-294.

Clarke, D.B., Upton, B.G.J. (1971) Tertiary Basalts of Baffin Island: Field Relations and Tectonic Setting. *Canadian Journal of Earth Sciences* 8, 248-258.

Han, P.-Y., Rudnick, R.L., He, T., Marks, M.A.W., Wang, S.-J., Gaschnig, R.M., Hu, Z.-C. (2023) Halogen (F, Cl, Br, and I) concentrations of the upper continental crust through time as recorded in ancient glacial diamictite composites. *Geochimica Et Cosmochimica Acta* 341, 28-45.

Herzberg, C., O'Hara, M.J. (2002) Plume-associated ultramafic magmas of phanerozoic age. *Journal of Petrology* 43, 1857-1883.

Jackson, M.G., Carlson, R.W., Kurz, M.D., Kempton, P.D., Francis, D., Blusztajn, J. (2010) Evidence for the survival of the oldest terrestrial mantle reservoir. *Nature* 466, 853-856.

298 Joachim, B., Pawley, A., Lyon, I.C., Marquardt, K., Henkel, T., Clay, P.L., Ruzie, L.,
299 Burgess, R., Ballentine, C.J. (2015) Experimental partitioning of F and Cl between
300 olivine, orthopyroxene and silicate melt at Earth's mantle conditions. *Chemical*
301 *Geology* 416, 65-78.
302 John, T., Layne, G.D., Haase, K.M., Barnes, J.D. (2010) Chlorine isotope evidence for
303 crustal recycling into the Earth's mantle. *Earth and Planetary Science Letters*
304 298, 175-182.
305 Kendrick, M.A., Arculus, R., Burnard, P., Honda, M. (2013a) Quantifying brine
306 assimilation by submarine magmas: Examples from the Galapagos Spreading
307 Centre and Lau Basin. *Geochimica Et Cosmochimica Acta* 123, 150-165.
308 Kendrick, M.A., Hémond, C., Kamenetsky, V.S., Danyushevsky, L., Devey, C.W.,
309 Rodemann, T., Jackson, M.G., Perfit, M.R. (2017) Seawater cycled throughout
310 Earth's mantle in partially serpentinized lithosphere. *Nature Geoscience* 10.
311 Kendrick, M.A., Honda, M., Pettke, T., Scambelluri, M., Phillips, D., Giuliani, A. (2013b)
312 Subduction zone fluxes of halogens and noble gases in seafloor and forearc
313 serpentinites. *Earth and Planetary Science Letters* 365, 86-96.
314 Kendrick, M.A., Jackson, M.G., Hauri, E.H., Phillips, D. (2015) The halogen (F, Cl, Br, I)
315 and H2O systematics of Samoan lavas: Assimilated-seawater, EM2 and high-
316 He-3/He-4 components. *Earth and Planetary Science Letters* 410, 197-209.
317 Kendrick, M.A., Jackson, M.G., Kent, A.J.R., Hauri, E.H., Wallace, P.J., Woodhead, J.
318 (2014) Contrasting behaviours of CO2, S, H2O and halogens (F, Cl, Br, and I) in
319 enriched-mantle melts from Pitcairn and Society seamounts. *Chemical Geology*
320 370, 69-81.
321 Kendrick, M.A., Nebel, O., Hanyu, T., Maunder, B.L., Maas, R. (2025) Earth's early
322 differentiation recorded by halogen abundance ratios in Hawaiian lavas.
323 *Geochimica Et Cosmochimica Acta* 393, 196-207.
324 Kent, A.J.R., Stolper, E.M., Francis, D., Woodhead, J., Frei, R., Eiler, J. (2004) Mantle
325 heterogeneity during the formation of the North Atlantic Igneous Province:
326 Constraints from trace element and Sr-Nd-Os-O isotope systematics of Baffin
327 Island picrites. *Geochemistry, Geophysics, Geosystems* 5.
328 Keppler, H. (2017) Fluids and trace element transport in subduction zones. 102, 5-20.
329 Larsen, L.M., Pedersen, A.K., Pedersen, G.K., Piasecki, S. (1992) Timing and duration of
330 Early Tertiary volcanism in the North Atlantic: new evidence from West
331 Greenland. *Geological Society, London, Special Publications* 68, 321-333.
332 Lass-Evans, S. (2004) Anatomy of the ancestral Iceland plume a chemical and isotopic
333 study of the tertiary basalts and picrites from Baffin Island, University of
334 Edinburgh.
335 Lodders, K., Fegley, B. (1998) The Solar System, *The Planetary Scientist's Companion*.
336 Pedersen, A.K., Larsen, L.M., Pedersen, G.K. (2017) Lithostratigraphy, geology and
337 geochemistry of the volcanic rocks of the Vaigat Formation on Disko and
338 Nuussuaq, Paleocene of West Greenland. *GEUS Bulletin* 39, 1-244.
339 Robillard, I., Francis, D., Ludden, J.N. (1992) The relationship between E- and N-type
340 magmas in the Baffin Bay Lavas. *Contributions To Mineralogy and Petrology* 112,
341 230-241.
342 Sharp, Z.D., Barnes, J.D., Brearley, a.J., Chaussidon, M., Fischer, T.P., Kamenetsky, V.S.
343 (2007) Chlorine isotope homogeneity of the mantle, crust and carbonaceous
344 chondrites. *Nature* 446, 1062-1065.

Starkey, N.A., Fitton, J.G., Stuart, F.M., Larsen, L.M. (2012) Melt inclusions in olivines from early Iceland plume picrites support high 3He/ 4He in both enriched and depleted mantle. *Chemical Geology* 306-307, 54-62.

Starkey, N.A., Stuart, F.M., Ellam, R.M., Fitton, J.G., Basu, S., Larsen, L.M. (2009) Helium isotopes in early Iceland plume picrites: Constraints on the composition of high 3He/4He mantle. *Earth and Planetary Science Letters* 277, 91-100.

Stroncik, N.A., Haase, K.M. (2004) Chlorine in oceanic intraplate basalts: Constraints on mantle sources and recycling processes. *Geology* 32, 945-948.

Stuart, F.M., Lass-Evans, S., Fitton, J.G., Ellam, R.M. (2003) High He-3/He-4 ratios in picritic basalts from Baffin Island and the role of a mixed reservoir in mantle plumes. *Nature* 424, 57-59.

Willhite, L.N., Jackson, M.G., Blichert-Toft, J., Bindeman, I., Kurz, M.D., Halldorsson, S.A., Hardardottir, S., Gazel, E., Price, A.A., Byerly, B.L. (2019) Hot and Heterogenous High-He-3/He-4 Components: New Constraints From Proto-Iceland Plume Lavas From Baffin Island. *Geochemistry Geophysics Geosystems* 20, 5939-5967.

Yuan, l., Steinle-Neumann, G. (2024) Earth's “missing” chlorine may be in the core. *Journal of Geophysical Research: Solid Earth* 129, e2023JB027731.

Table and Figure captions

Sample	CS-5		CS-6		PI-25		362077		332901	
Location	Cape Searle, Baffin Island		Cape Searle, Baffin Island		Padloping, Baffin Island		Nuussuaq, West Greenland		Disko, West Greenland	
Member	Anaanaa		Anaanaa		Anaanaa		Naujánguit		Ordlingassoq	
Deg. N	67.22		67.22		67.18		70.50		70.38	
Deg. W	62.53		62.53		62.45		53.57		53.22	
Emplacement[$]	Dyke		Dyke		Subaerial lava flow		Submarine pillow lava		Subaerial lava flow	
Olivine Fo	84.8 *(1.2)*		84.5 *(0.2)*		84.5 *(01.0)*		81.1 *(6.8)*		86.0 *(1.6)*	
Type	E		E		N		N		E	
$^{3}He/^{4}He$ (R/R_a)*	26.30	*(2.0)*	37.90	*(1.2)*	49.50	*(1.6)*	44.00	*(0.8)*	45.80	*(1.0)*
n	8		3		32		4		2	
SiO_2 (wt%)	51.38	*(3.30)*	49.06	*(1.81)*	49.84	*(1.51)*	49.64	*(2.13)*	52.96	*(0.51)*
Al_2O_3 (wt%)	17.57	*(2.46)*	15.45	*(0.34)*	15.39	*(0.90)*	15.85	*(0.93)*	15.64	*(0.01)*
TiO_2 (wt%)	1.41	*(0.27)*	1.30	*(0.05)*	1.21	*(0.36)*	1.30	*(0.10)*	1.98	*(0.17)*
FeOt (wt%)	7.90	*(2.48)*	10.04	*(0.08)*	9.98	*(0.91)*	8.88	*(4.40)*	5.99	*(0.30)*
MnO (wt%)	0.16	*(0.13)*	0.18	*(0.03)*	0.19	*(0.10)*	0.17	*(0.09)*	0.12	*(0.04)*
MgO (wt%)	3.17	*(2.88)*	7.65	*(0.77)*	7.50	*(1.17)*	7.26	*(2.52)*	7.75	*(0.03)*
CaO (wt%)	14.99	*(1.58)*	12.77	*(1.30)*	13.19	*(0.67)*	13.08	*(1.77)*	12.38	*(0.30)*
Na_2O (wt%)	2.03	*(0.93)*	2.00	*(0.10)*	2.06	*(0.25)*	2.04	*(0.07)*	2.64	*(0.17)*
K_2O (wt%)	0.29	*(0.14)*	0.35	*(0.18)*	0.21	*(0.10)*	0.34	*(0.11)*	0.54	*(0.01)*
Total	98.88		98.80		99.56		98.56		99.98	
n F/Cl/Br	4/4/0		2/3/3		11/11/4		1/3/4		2/3/2	
F ($\mu g.g^{-1}$)	211	*(26)*	174	*(168)*	174	*(28)*	216	*NA*	440	*(14)*
Cl ($\mu g.g^{-1}$)	100	*(22)*	78	*(17)*	85	*(32)*	98	*(31)*	83	*(42)*
Br ($ng.g^{-1}$)	<LOD	*NA*	530	*(439)*	961	*(371)*	1133	*(782)*	905	*(366)*
K/Cl	27	*(14)*	42	*(13)*	25	*(18)*	31	*(10)*	62	*(27)*
F/Cl	2.1	*(0.3)*	2.4	*(2.4)*	2.1	*(0.6)*	2.1	*NA*	5.7	*(3.8)*
1000Br/Cl	-	-	6.7	*(5.0)*	11.8	*(4.9)*	11.8	*(5.9)*	12.4	*(0.7)*
n	4		1		12		-		-	
$d^{37}Cl$ (‰)	0.60	*(0.21)*	0.04	*(0.43)*	-0.21	*0.64*	-	-	-	-

Table 1: Average composition of PIP melt inclusions. [$]Emplacement information from LASS-EVANS (2004), and PEDERSEN *et al.* (2017), *He data from STUART *et al.* (2003) and STARKEY *et al.* (2009). Uncertainties are 2σ.

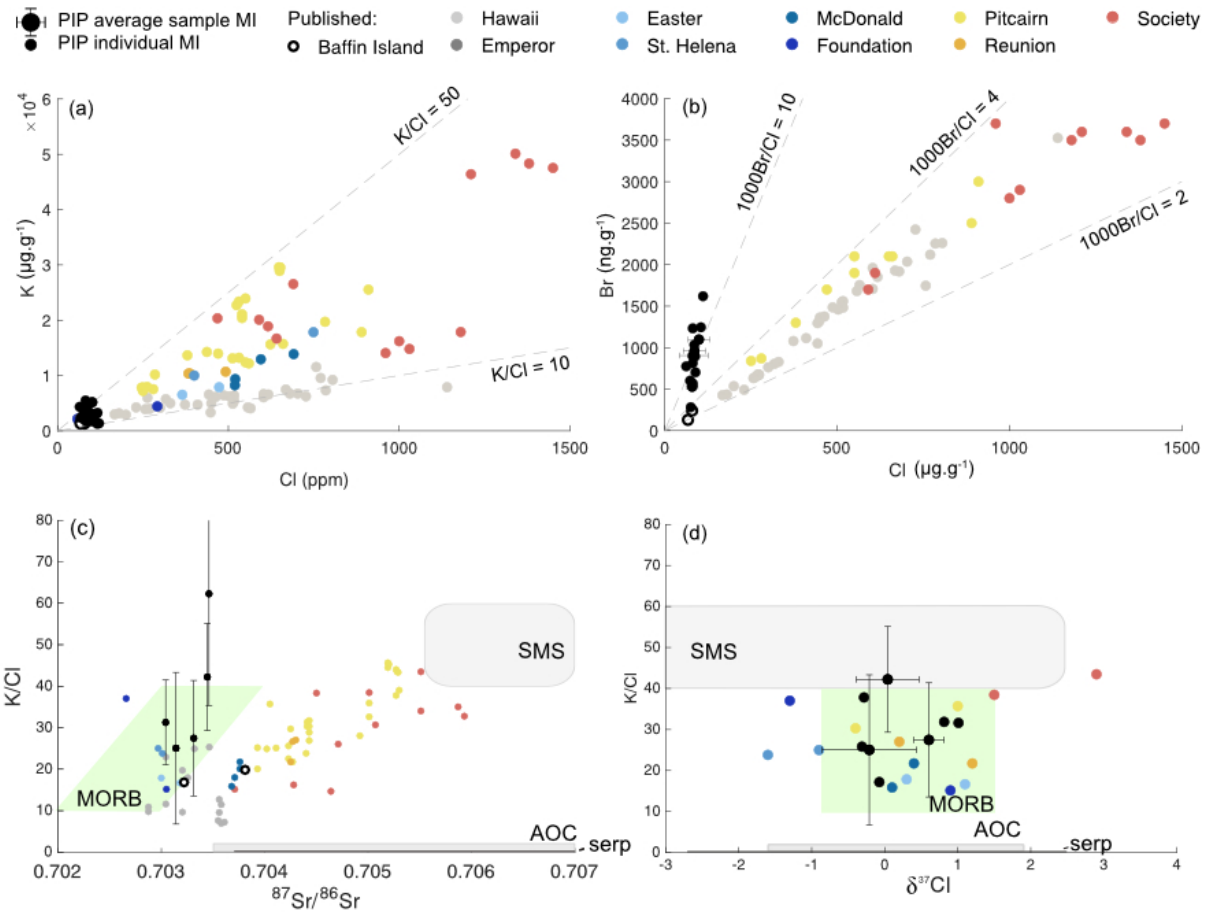

Figure 1: Compositions of the melt inclusions in PIP basalt olivine compared to glasses from depleted (grey; BROADLEY *et al.,* 2019, Kendrick *et al.,* 2025), EM-type (warm colours; STRONCIK AND HAASE 2004; JOHN *et al.,* 2010) and HIMU (blues; STRONCIK AND HAASE, 2004; JOHN *et al.*, 2010; KENDRICK *et al.*, 2014) basalts. MORB (green field) is from KENDRICK *et al.* (2017). Data sources for average SMS (subducted marine sediments), AOC (altered oceanic crust) and serpentinite fields are provided in table S-4.

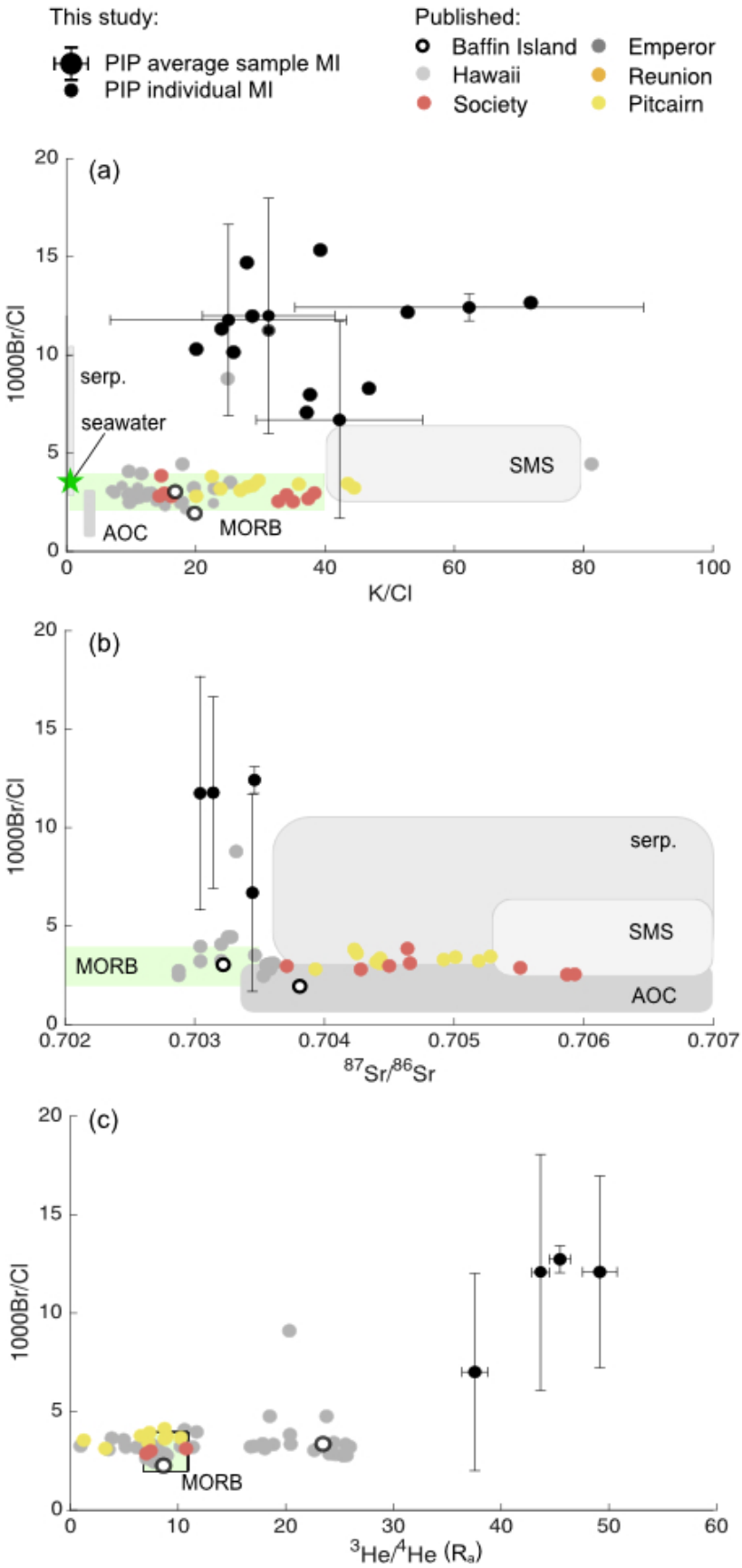

Figure 2: Composition of melt inclusions in PIP olivines compared to depleted (grey), EM-type (warm colours) and HIMU (blues) OIB and to MORB (green field). Date sources as in figure 1.

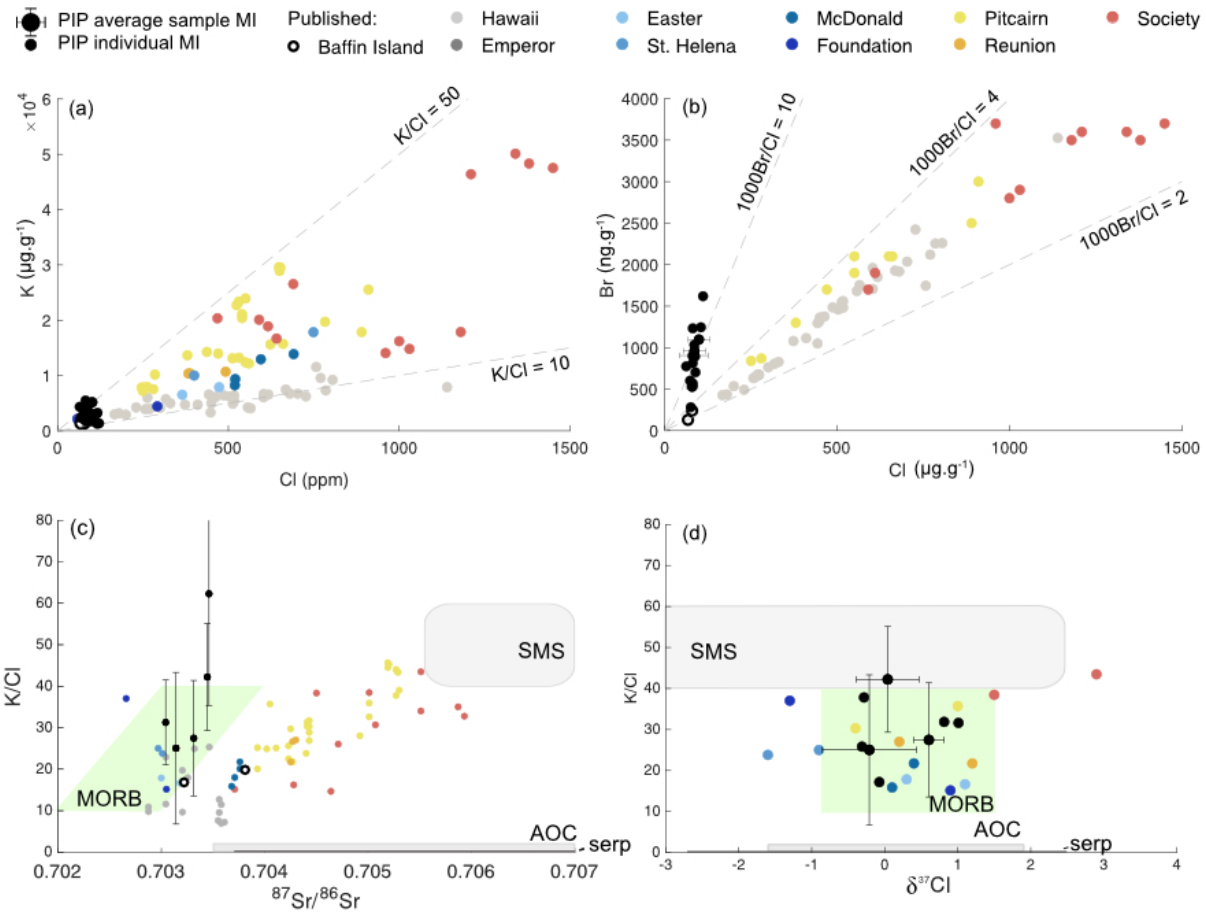

Figure 3: Calculated accumulated fractional melting path yielding the melt seen in N-type (PI-25), and E-type (CS-6) PIP basalts, shown in increments of F=0.1 from 0.1 (PI-25) and 0.25 (CS-6). Compared to estimates for DM, BSE and to peridotite xenoliths from intraplate settings and to CI- and CM-chondrites (table S-6).

Geochemical Perspectives Letters

Halogens in proto-Iceland plume basalts

E.L. Tomlinson, E.F. Rose-Koga, A-S Bouvier, D. O'Farrell, J.T. Caulfield, M.G. Jackson, Y. Moussallam, F.M. Stuart, J. Villeneuve

Supplementary Information

- Methods
- Major element composition
- Halogen partitioning calculation
- Tables S-1 to S-6
- Figure S-1 to S-4
- Supplementary Information References

Methods

Sample preparation

Olivine crystals from the selected PIP lava flows are medium sized (300-500 µm) equant and tabular crystals. Olivine grains containing melt inclusions were hand-picked under transmitted light at 50-100× magnification, care was taken to avoid inclusions that were open or connected to cracks or spinel mineral inclusions. Melt inclusions are rounded, optically clear to pink glasses, ranging in size from 20 to 100 µm (Fig. S-1). Where possible, we selected clean, glassy inclusions. Melt inclusions in sample 332901 were re-homogenised using a Vernadsky-type microscope heating stage at 1-atm (Sobolev *et al.*, 1980; Schiano, 2003) following the procedure described in Le Voyer *et al.* (2010). In short, a partially crystallized melt inclusion is put in a 1-atm oven in which the oxygen fugacity is kept low at 10^{-10} atm with purified He with Zr at 700ºC to avoid oxidation of the host crystal and to facilitate a rapid quench. We increased the temperature at a rate of about 8ºC/min and visually monitored the regular disappearance of crystals in the melt inclusion. Once all crystals had melted inside the melt inclusion, we kept the temperature constant for 5 more minutes and then quenched the experiment. The heating procedure was completed in less than 30 minutes. Selected olivine grains were mounted onto individual glass slides using Crystalbond 509 and then individually polished by hand using progressively fining grit SiC papers and then diamond paste to expose the melt inclusions. The melt inclusion-bearing olivines were liberated from the Crystalbond and mounted in a Struers Epofix resin mount before receiving a final ¼ µm diamond paste polish on an automated polisher. The mount was then analysed for major elements and chlorine isotopes. The melt inclusion-bearing olivine grains were then liberated from the epoxy mount and cleaned in acetone and distilled water before being pressed into indium (Rose-Koga *et al.*, 2021) for elemental halogen analysis by SIMS.

Major element analysis (EMPA-WDS and SEM-EDX)

Major element compositions of PIP melt inclusions were analysed using a JEOL 8600 electron microprobe equipped with 4 wavelength dispersive spectrometers (EMPA-WDS) at the Research Laboratory for Archaeology and the History of Art (RLAHA), University of Oxford. Data were acquired at an accelerating voltage of 15 KeV, a beam current of 5 nA and a beam diameter of 5 µm. Peak count times were 30-70 s on each peak except for Na (12 s). The instrument was calibrated for the beam conditions using a suite of appropriate mineral standards and count rates were corrected using the PAP absorption correction method. Volatile elements were also analysed by EMPA-WDS at the RLAHA. Analyses used peak counting times of 120 s for F, P and S and 30 s for Cl, however both F and Cl were below the detection limits of 0.11 and 0.03 %, respectively.

	Crystal	Peak count time (s)	Background count time either side of peak (s)
Na	TAP	12	6
Mg	TAP	70	35
Al	TAP	50	25
Si	TAP	30	15
K	PET	30	15
Ca	PET	30	15
Ti	PET	30	15
Mn	LIF	40	20
Fe	LIF	40	20
F	LDE	120	60
P	TAP	120	60
Cl	PET	30	15
Cr	PET	60	30
S	PET	120	120

Additional major element analyses were undertaken at the iCRAG laboratory at Trinity College Dublin using a using a Tescan Mira XMU field-gun emission scanning electron microscope equipped with an XMAX 80 nm^2 energy dispersive (SEM-EDS) detector. Measurements were conducted using an accelerating voltage of 20 kV and a beam current of 300 pA. A suite of appropriate mineral standards from the Smithsonian Institute (JAROSEWICH *et al.*, 1980) was used to calibrate the instrument for quantitative analyses. Totals acquired were all within ±1 % of 100 wt%. Both EMPA-WDS and SEM-EDS methods were verified using the StHs6/80-G and GOR128-G MPI-DING reference glasses from the Max Planck Institute (Jochum *et al.*, 2006) and accuracy (%bias) and precision (%RSD) are typically better than ±5 % for both methods for all elements at concentrations above 0.5 wt%. Data is provided in table S-1.

Elemental halogen analysis

Halogen concentrations of PIP melt inclusions were analysed by secondary ion mass spectrometry (SIMS) using a CAMECA ims1280-HR at Centre de Recherches Pétrographiques et Géochimiques. The samples were sputtered with a Cs^+ primary beam at an accelerating voltage of 10 kV and focused as a 15 µm beam size on the sample. Each spot was sputtered either for 300 sec with a 6µm rastered beam of 0.5 nA in 2022 or

for 60 sec with a 5µm rastered beam of a stronger primary intensity of 3nA in 2019. The electron gun was used for charge compensation at the surface of the sample. Negative secondary ions were extracted through a potential of 10 kV and measured in peak jumping mode on several EM detectors. Analytical conditions are shown below.

For analysis of Br, energy filtering was set between +20 to +30 eV to reduce matrix effects. The mass resolving power was set to about 21,000 to separate mass interferences from hydrides (SeH), oxides (CuO) and metals (FeMg, VMg, CrAl and FeAl) on Br. In the 2019 session, Br concentrations were measured in a dedicated Br analysis in which we measured masses 76.85 (background), 77 ($^{29}Si^{16}O_3$), 78 ($^{30}Si^{16}O_3$), 79 (Br) and 81 (Br); these masses were selected to minimize the hysteresis of the magnet. In 2022, we measured Br in the same analysis as F and Cl, so we measured mass ^{79}Br, and ^{81}Br in addition to 17.8 (background), ^{18}O, ^{19}F, ^{27}Al, ^{30}Si, ^{35}Cl and ^{79}Br and ^{81}Br, we used a long wait time of 4s before analysis of ^{79}Br to allow the magnet to settle.

Halogen analyses were calibrated using a suite of natural basalt glasses: VG-2, also known as USNM 111240/52 (Straub and Layne, 2003; Rose-Koga et al., 2020) and Macquarie basalt glasses 25603, 40428, 47963 and 60701 (Kendrick et al., 2012; Kendrick et al., 2017). The reference values for these glasses and the measured raw counts are summarised in table S-2 and the resulting calibration curves are shown in figure S-2. We measured both ^{79}Br and ^{81}Br (Fig. S-3), however we use ^{79}Br to quantify Br in the studied samples as this reproduced the known Br contents of the quality control standards more closely. All errors are quoted as 2σ and include both the analytical uncertainty and the propagated error on the calibration curve.

Date	10-11 April 2019 Br	12 April 2019 Volatile elements	11-12 July 2022 Halogens
Masses	76.85 (background) $^{29}Si^{16}O_3$, $^{30}Si^{16}O_3$, ^{79}Br, ^{81}Br	11.8 (background FC), 11.9 (background EM) ^{12}C, ^{17}O, $^{16}O^1H$, ^{18}O, ^{19}F, ^{27}Al, ^{30}Si, ^{32}S, ^{35}Cl,	17.8O (background) ^{18}O, ^{19}F, ^{27}Al, ^{30}Si, ^{35}Cl, ^{79}Br, ^{81}Br,
Energy filtering	20 eV	20 eV	30 eV
Primary beam current	3.4 nA	1 nA	0.5 nA
Pre sputter	60 s	60 s	300 s
Raster area	5 x 5 µm	10 x 10 µm	6 x 6 µm
MRP	21000	7500	22000
Analysis time	4 s (background) 4 s, 4 s, 12 s, 12 s	2 s, 1 s (background) 4s, 2s, 4s, 4s, 2s, 2s, 4s, 4s, 3s	4 s (background) 3 s, 5 s, 3 s, 3 s, 4 s, 10 s, 10 s
Wait time before	2 s for all	2 s, 1 s (background) 1 s for all	4 s (background) 1 s, 1 s, 1 s, 1 s, 1 s, 4 s, 2 s
No. cycles	12	10	10
Approx. analysis time	12 minutes	18 minutes	18 minutes

The limit of determination was calculated from the calibration curve using the formula LoD = 3.33 × σ/S, where σ is the standard deviation of the intercept and S is the slope of the calibration curve. Measured reference material compositions are provided in table S-1. Accuracy is typically better than ±10 %bias for Cl in MPI-DING glasses StHs6/80-G and KL2-G, while the measured concentrations of F in both glasses are slightly low but are within error of the reference values reported by Jochum et al. (2006). For Br, accuracy is typically better than ±10 %bias for StHs6/80-G (0.8 ± 0.2 µg.g^{-1}; Jochum et al., 2006), but is worse in KL2-G (0.2 µg.g^{-1}; Jochum et al., 2006) at +30 %bias, suggesting that Br concentration may be overestimated at

low abundance. This is particularly true for the 2019 Br data which should be treated with caution as no other Br quality control standard was analysed in this session. Precision for repeat analysis of F, Cl and Br in MPI-DING glass StHs6/80-G is typically better than ±15 %RSD.

Errors on individual halogen analyses are derived from uncertainty on the linear fit of the appropriate calibration curve and errors on halogen ratios for individual melt inclusions are determined by propagating this calibration uncertainty. For the studied melt inclusions, absolute halogen concentrations may be affected by post entrapment crystallisation (see below), therefore we calculate halogen ratios for individual inclusions where both elements were measured, the average sample values are then the averages of those ratios in melt inclusions from olivines from a given sample lava flow.

Chlorine isotopic analysis

Chlorine isotope compositions were analysed in 2017 using a CAMECA ims1280-HR at the SwissSIMS laboratory, University of Lausanne following a method similar to that of Manzini *et al.* (2017). Samples were sputtered with a 1.5 nA Cs^+ primary beam with an accelerating voltage of 10kV, initially the beam was rastered over an area of 25 µm for 250 s to remove surface Cl contamination. Each analysis consists of 70 cycles of 10 sec, using a rastered beam over an area of 10 µm. It results of a total time per analysis of 17 minutes, included automated centring of the secondary beam in field and contrast apertures. Secondary ions were extracted into the mass spectrometer through a potential of 10 kV, through an energy slit set to a width of 50 eV and were counted on two electron multiplier detectors simultaneously. The mass resolving power was set to ~4800. Glass standards B-21, B-20D (basalts; John *et al.*, 2010) were used for calibration, B-20D was closest to the sample glass composition and so was used to correct for mass fractionation. Additionally, StHs6/80-G and T1-G (andesite and granodiorite; Jochum *et al.*, 2006), for which no bulk $\delta^{37}Cl$ value exists but was proven to give reproducible data, was used to monitor the instrument stability. A drift correction was applied for mount 2 where 4 permil shift was observed for StHs6/80-G. Reproducibility of the StHs6/80-G after drift correction was ~0.4 permil (2 σ). Errors of individual analysis are calculated as two standard errors of the 70 cycles and depends on the Cl content (correlated to count rate) of each melt inclusion compositions.

Major element compositions

Host olivines have magnesian cores with forsterite (Fo, Mg/Mg+Fe) of 86-87, most of the studied samples span a fairly narrow compositional range with only weak normal zoning towards their rims (Fo_{83}-Fo_{85}), however olivines from sample 332901 extend to lower forsterite contents (Fo_{76}). The observed forsterite contents are comparable to the composition of olivine expected to be in equilibrium with sample DUR1, a phenocryst-poor lava sample considered to be the most unfractionated of the PIP lavas (Starkey *et al.*, 2012). The olivines have CaO contents of 0.26-0.37 wt%. High-Mg PIP olivines are considered phenocrysts, rather than xenoliths from the peridotite mantle, because they show smooth continuous trends in Cr_2O_3 and CaO over the range of forsterite, consistent with derivation from the same magmatic system (Larsen and Pedersen, 2000; Starkey *et al.*, 2012). In addition, PIP olivines are characterised by higher CaO for a given forsterite content than olivine from mantle xenoliths from West Greenland (Bernstein *et al.*, 2006), consistent with a high-temperature, low pressure magmatic origin (Jackson and Shirey, 2011).

The melt inclusions have MgO 2.7-8.7 wt%. This is lower than the whole-rock compositions of their host lavas reported by (STARKEY *et al.*, 2009), suggesting that they have undergone post entrapment crystallisation (PEC) during which the encapsulated melt crystallises olivine at the inclusion/phenocryst interface during cooling e.g. (Sobolev, 1996). Indeed, thin recrystallisation rims are observed in back-scattered electron images of the majority of inclusions. To calculate the liquid line of decent (LLD) of the

melt inclusions, equilibrium olivine was subtracted in 0.1 % increments from the whole rock composition of DUR1, a phenocryst poor PIP lava considered to represent the liquid composition (Starkey *et al.*, 2012). The composition of equilibrium olivine was calculated using an equilibrium constant $K_D = 0.3$ (Roedder and Emslie, 1970). Four of the samples, those with glassy melt inclusions, lie on the calculate LLD, suggesting their compositions are consistent with perfect fractional crystallisation of 2-10 % (PI-25, CS-6 and 362077) and 5-25% (CS-5) olivine (Fig. S-4). For samples in which melt inclusions show small degrees of PEC (5-10 %), melt inclusions show a limit range of major element and halogen compositions. The highest K and Cl contents are found in melt inclusions with the lowest MgO, consistent with evolution on the LLD during PEC of olivine.

Sample 332901 lies off the LLD and has melt compositions suggesting diffusive equilibration between the trapped melt and the host olivine, melt inclusions in this sample were originally crystalised and were homogenised for this study. We have not corrected for PEC because although the halogens are incompatible element during olivine crystallisation and their concentrations will increase in the melt, their ratios in the melt will be unchanged at F>0.1, which is the minimum degree of melting proposed for the PIP source by Herzberg and O'Hara (2002).

Halogen partition calculation

Experimental work demonstrates that F is more compatible than Cl in mantle minerals and that both become less incompatible with increasing temperature (Joachim *et al.*, 2015). We use partition coefficients determined at 1500°C and 2.3 GPa, conditions appropriate for partial melting in the OIB source mantle (DASGUPTA *et al.*, 2007). We use D_F^{ol}, D_F^{opx}, D_{Cl}^{ol}, and D_{Cl}^{opx} at 1500 °C from figure 4 of Joachim *et al.* (2015). Following Joachim *et al.* (2015) and based on the lower temperature datasets of Hauri *et al.* (2006); Dalou *et al.* (2012); Dalou *et al.* (2014), we assume that D_F^{cpx}/D_F^{opx} is 1.5 and $D_{Cl}^{cpx}/D_{Cl}^{opx}$ is 5. Following KENDRICK *et al.* (2012) we assume that Br and Cl are similarly incompatible ($D_{Br} = D_{Cl}$) in olivine, orthopyroxene and clinopyroxene. In practice, Br may be less compatible than Cl on account of its larger ionic radius, however even if the partition coefficient of Br is two orders lower than that of Cl, this will only affect the calculated composition of the source below ~F=0.1, lower than the degree of melting for both E and N-type PIP magmas proposed by Herzberg and O'Hara (2002). Table S-5 shows the average modal abundances of olivine, orthopyroxene and clinopyroxene in spinel peridotites (McDonough, 1990), excluding minor garnet/spinel, along with the mineral and resulting bulk F, Br and Cl partition coefficients used for accumulated fractional melting modelling. Table S-6 shows the calculated compositions of the PI-25 and CS-6 source regions compared to estimates for the depleted mantle (DM) and bulk silicate Earth (BSE) and data for intraplate lithospheric xenoliths.

Supplementary Tables

Table S-1 Major element, elemental halogen, chlorine isotope compositions of PIP melting inclusions, along with major element compositions of host olivine and published whole rock trace element and isotope compositions.

Table S-2 Raw data and reference values used for calibration of F, Cl and Br. Reference values are from: VG-2, also known as USNM 111240/52 (Straub and Layne, 2003; Rose-Koga et al., 2020) and Macquarie basalt glasses 25603, 40428, 47963 and 60701 (Kendrick et al., 2012; Kendrick et al., 2017). Errors on reference values are 2σ. NA – data not available. The limit of determination calculated for each session is also shown.

	F			Cl			Br				
	$^{19}F/^{30}Si$	Error (σ)	F (μg.g^{-1})	$^{35}Cl/^{30}Si$	Error (σ)	Cl (μg.g^{-1})	$^{81}Br/^{30}Si$	Error	$^{79}Br/^{30}Si$	Error	Br (μg.g^{-1})
12/07/2022											
VG2	1.76E-01	1.09E-02	334 ± 14	2.68E-01	1.65E-02	306 ± 13	4.14E-04	1.98E-05	2.95E-04	1.55E-05	NA
VG2	1.85E-01	2.03E-02	334 ± 14	2.57E-01	1.52E-02	306 ± 13	3.92E-04	2.44E-05	2.86E-04	1.99E-05	NA
VG2	1.86E-01	1.28E-02	334 ± 14	2.54E-01	1.42E-02	306 ± 13	3.59E-04	2.26E-05	2.49E-04	1.72E-05	NA
25603	6.09E-01	2.96E-02	769	7.00E-01	3.94E-02	799 ± 17	7.80E-04	4.89E-05	6.10E-04	3.96E-05	2.64 ± 0.06
25603	7.16E-01	4.25E-02	769	7.19E-01	4.84E-02	799 ± 17	7.95E-04	3.89E-05	5.57E-04	2.93E-05	2.64 ± 0.06
25603	5.62E-01	3.12E-02	769	6.91E-01	4.63E-02	799 ± 17	7.85E-04	4.94E-05	5.67E-04	3.67E-05	2.64 ± 0.06
60701	4.69E-01	4.13E-02	536	3.55E-01	2.02E-02	435 ± 10	3.98E-04	1.99E-05	2.42E-04	1.34E-05	1.38 ± 0.04
60701	3.93E-01	3.18E-02	536	3.48E-01	1.97E-02	435 ± 10	4.16E-04	3.03E-05	2.27E-04	1.83E-05	1.38 ± 0.04
60701	4.01E-01	1.60E-02	536	3.51E-01	1.96E-02	435 ± 10	3.97E-04	2.56E-05	2.31E-04	1.52E-05	1.38 ± 0.04
40428	6.59E-01	5.02E-02	729	4.45E-01	2.44E-02	494 ± 11	4.27E-04	2.17E-05	2.72E-04	1.90E-05	1.58 ± 0.04
40428	6.33E-01	3.37E-02	729	4.49E-01	2.60E-02	494 ± 11	4.56E-04	3.04E-05	2.61E-04	1.79E-05	1.58 ± 0.04
40428	4.35E-01	3.16E-02	729	4.44E-01	2.49E-02	494 ± 11	4.65E-04	3.07E-05	5.04E-04	3.35E-05	1.58 ± 0.04
47963	1.16E+00	8.40E-02	1262	1.22E+00	8.14E-02	1356 ± 30	1.23E-03	7.29E-05	1.02E-03	6.11E-05	4.57 ± 0.11
47963	1.08E+00	6.33E-02	1262	1.06E+00	6.89E-02	1356 ± 30	1.27E-03	7.93E-05	7.58E-04	4.93E-05	4.57 ± 0.11
LoD (μg.g^{-1})	64			51			0.13		0.49		
13/07/2022											
47963	1.19E+00	9.10E-02	1262	1.05E+00	6.33E-02	1356 ± 30	1.23E-03	6.97E-05	1.29E-03	7.33E-05	4.57 ± 0.11
47963	1.08E+00	6.74E-02	1262	9.28E-01	4.60E-02	1356 ± 30	1.28E-03	6.83E-05	1.31E-03	6.86E-05	4.57 ± 0.11
60701	4.62E-01	3.60E-02	536	2.76E-01	1.51E-02	435 ± 10	4.38E-04	1.93E-05	3.86E-04	1.89E-05	1.38 ± 0.04
60701	6.51E-01	3.86E-02	536	3.15E-01	1.39E-02	435 ± 10	4.66E-04	2.57E-05	4.19E-04	2.46E-05	1.38 ± 0.04
60701	6.81E-01	3.70E-02	536	3.25E-01	1.76E-02	435 ± 10	4.44E-04	2.63E-05	3.99E-04	2.43E-05	1.38 ± 0.04
60701	5.07E-01	3.00E-02	536	3.35E-01	1.82E-02	435 ± 10	4.36E-04	2.56E-05	3.92E-04	2.36E-05	1.38 ± 0.04
25603	6.53E-01	3.07E-02	769	5.92E-01	2.47E-02	799 ± 17	7.92E-04	5.00E-05	7.74E-04	4.92E-05	2.64 ± 0.06
25603	5.45E-01	6.55E-02	769	5.87E-01	3.60E-02	799 ± 17	8.01E-04	4.35E-05	7.85E-04	4.36E-05	2.64 ± 0.06
25603	7.06E-01	4.88E-02	769	6.32E-01	3.78E-02	799 ± 17	7.45E-04	4.34E-05	7.65E-04	4.56E-05	2.64 ± 0.06
25603	6.37E-01	4.66E-02	769	6.16E-01	3.51E-02	799 ± 17	7.27E-04	3.04E-05	7.50E-04	3.21E-05	2.64 ± 0.06
VG2	2.29E-01	1.45E-02	334 ± 14	2.24E-01	1.20E-02	306 ± 13	4.20E-04	2.29E-05	4.71E-04	2.62E-05	NA
VG2	2.44E-01	9.64E-03	334 ± 14	2.39E-01	1.33E-02	306 ± 13	3.91E-04	2.08E-05	4.45E-04	2.45E-05	NA
VG2	2.07E-01	1.33E-02	334 ± 14	1.95E-01	9.46E-03	306 ± 13	3.74E-04	1.71E-05	3.82E-04	2.00E-05	NA
VG2	1.93E-01	9.13E-03	334 ± 14	2.23E-01	1.19E-02	306 ± 13	3.95E-04	2.03E-05	4.36E-04	2.42E-05	NA
LoD (μg.g^{-1})	113			49			0.19		0.07		

Continues over…

	F			Cl			Br				
	^{19}F /^{30}Si	Error (σ)	F (µg.g^{-1})	^{35}Cl /^{30}Si	Error (σ)	Cl (µg.g^{-1})	^{81}Br /$^{30}SiO_3$	Error	^{79}Br/$^{30}SiO_3$	Error	Br (µg.g^{-1})
11/04/2019											
47963							3.70E-02	7.32E-04	3.52E-02	8.02E-04	4.57 ± 0.11
47963							3.65E-02	7.49E-04	3.52E-02	7.99E-04	4.57 ± 0.11
25603							2.31E-02	4.62E-04	2.03E-02	6.92E-04	2.64 ± 0.06
25603							2.30E-02	5.42E-04	2.05E-02	4.04E-04	2.64 ± 0.06
25603							2.32E-02	4.24E-04	1.92E-02	4.58E-04	2.64 ± 0.06
60701							1.60E-02	3.69E-04	1.24E-02	2.90E-04	1.38 ± 0.04
60701							1.59E-02	1.83E-04	1.25E-02	3.76E-04	1.38 ± 0.04
LoD (µg.g^{-1})							0.38		0.18		
12/09/2019											
47963	3.27E+00	1.77E-02	1262	1.99E+00	1.44E-02	1356 ± 30					
47963	3.26E+00	1.88E-02	1262	1.98E+00	1.60E-02	1356 ± 30					
47963	3.26E+00	2.11E-02	1262	1.98E+00	1.44E-02	1356 ± 30					
40428	1.89E+00	1.27E-02	729	7.01E-01	5.67E-03	494 ± 11					
40428	1.89E+00	1.14E-02	729	7.00E-01	4.21E-03	494 ± 11					
40428	1.89E+00	1.20E-02	729	6.97E-01	4.85E-03	494 ± 11					
VG2	6.34E-01	2.98E-03	334 ± 14	3.93E-01	2.30E-03	306 ± 13					
VG2	6.32E-01	3.72E-03	334 ± 14	4.00E-01	2.59E-03	306 ± 13					
VG2	6.46E-01	2.64E-03	334 ± 14	4.11E-01	2.97E-03	306 ± 13					
40428	1.89E+00	1.31E-02	729	6.99E-01	4.89E-03	494 ± 11					
40428	1.88E+00	1.27E-02	729	6.95E-01	4.61E-03	494 ± 11					
VG2	6.36E-01	4.66E-03	334 ± 14	4.12E-01	2.87E-03	306 ± 13					
VG2	6.27E-01	4.33E-03	334 ± 14	3.89E-01	2.16E-03	306 ± 13					
VG2	6.26E-01	4.47E-03	334 ± 14	4.01E-01	3.10E-03	306 ± 13					
47963	3.27E+00	1.96E-02	1262	2.01E+00	1.45E-02	1356 ± 30					
47963	3.26E+00	1.97E-02	1262	1.99E+00	1.72E-02	1356 ± 30					
47963	3.26E+00	1.74E-02	1262	2.00E+00	1.23E-02	1356 ± 30					
LoD (µg.g^{-1})	44			13							

Table S-3 Raw data and drift correction for calibration of δ^{37}Cl. Reference values for B2-1 and B20D are +0.59 ‰ (± 0.33 ‰) and +0.95 ‰ (± 0.33 ‰), respectively (JOHN *et al.*, 2010). MI – melt inclusion.

		^{37}Cl/^{35}Cl		^{35}Cl/Coeff		^{37}Cl/Coeff		yield	$\delta^{37}Cl$ raw		raw value		$\delta^{37}Cl$ corrected	
	(nA)	*H2/L1*	*1se*	*L1*	*1se*	*H2*	*1se*	*^{37}Cl cps/nA*	‰	*2se*	*bias to StH*	*IMF*	‰	*2se*
Reference material mount														
TiG	1.76	3.281E-01	2.15E-02	1.271E+05	9.489E-01	4.171E+04	9.44E-01	7.227E+04	26.64	0.43				
TiG	1.76	3.281E-01	2.16E-02	1.268E+05	8.773E-01	4.160E+04	8.81E-01	7.194E+04	26.59	0.43				
B2-1	1.76	3.265E-01	1.12E-02	1.014E+06	7.138E-01	3.311E+05	7.22E-01	5.768E+05	21.46	0.22	-6.24			
B2-1	1.75	3.267E-01	1.20E-02	9.984E+05	5.781E-01	3.262E+05	5.88E-01	5.697E+05	22.15	0.24	-5.56			
B20D	1.75	3.268E-01	1.04E-02	7.552E+05	5.053E-01	2.468E+05	5.13E-01	4.326E+05	22.52	0.21	-5.19	22.02		
B20D	1.74	3.269E-01	9.21E-03	7.081E+05	6.404E-01	2.314E+05	6.44E-01	4.066E+05	22.71	0.18	-4.99	22.21		
StH	1.73	3.283E-01	1.42E-02	2.943E+05	5.678E-01	9.664E+04	5.68E-01	1.699E+05	27.29	0.28				
StH	1.73	3.286E-01	1.45E-02	2.818E+05	5.442E-01	9.260E+04	5.45E-01	1.631E+05	28.13	0.29				
SC	1.72	2.803E-01	8.84E-01	4.960E+03	2.193E-01	1.391E+03	8.60E-01	2.880E+03	-122.86	17.67	blank			
Sample mount 1														
StH_mount1	1.69	3.285E-01	1.45E-02	2.806E+05	6.061E-01	9.217E+04	6.06E-01	1.656E+05	27.88	0.29	drift monitor			
CS5-3	1.70	3.269E-01	1.94E-02	1.575E+05	5.628E-01	5.148E+04	5.65E-01	9.269E+04	22.93	0.39			0.81	0.44
CS5-4	1.70	3.269E-01	2.05E-02	1.598E+05	5.016E-01	5.223E+04	5.13E-01	9.420E+04	22.79	0.41			0.67	0.46
bg_mount1	1.69	3.145E-01	2.94E-01	5.525E+03	1.610E+00	1.729E+03	1.31E+00	3.263E+03	-16.08	5.88	background			
CS5-5S	1.69	3.266E-01	2.27E-02	1.381E+05	4.428E-01	4.510E+04	4.50E-01	8.189E+04	22.04	0.45			-0.07	0.49
CS5-5L	1.68	3.270E-01	2.06E-02	1.388E+05	4.596E-01	4.538E+04	4.59E-01	8.258E+04	23.13	0.41			1.01	0.46
StH_mount1	1.67	3.285E-01	1.49E-02	2.847E+05	5.654E-01	9.353E+04	5.67E-01	1.704E+05	27.97	0.30	Drift monitor			
CS6-1	1.67	3.267E-01	2.13E-02	1.303E+05	4.266E-01	4.256E+04	4.31E-01	7.787E+04	22.16	0.43			0.04	0.47
Sample mount 2														
StH_mount2	1.65	3.285E-01	1.44E-02	2.835E+05	7.090E-01	9.315E+04	7.08E-01	1.723E+05	27.95	0.29	drift monitor			
PI-25_MI5	1.65	3.266E-01	2.12E-02	1.315E+05	5.735E-01	4.294E+04	5.78E-01	7.988E+04	21.99	0.42			-0.97	0.46
PI-25_MI7	1.64	3.273E-01	2.31E-02	1.453E+05	5.797E-01	4.758E+04	5.85E-01	8.853E+04	24.13	0.46			0.21	0.50
StH_mount2	1.63	3.292E-01	1.57E-02	2.799E+05	6.887E-01	9.213E+04	6.92E-01	1.712E+05	30.07	0.31	drift monitor			
bg_mount2	1.63	3.200E-01	2.88E-01	3.982E+03	9.707E-02	1.272E+03	3.36E-01	2.438E+03	1.43	5.77	background			
PI-25_MI9	1.63	3.275E-01	2.06E-02	1.387E+05	6.249E-01	4.542E+04	6.26E-01	8.517E+04	24.60	0.41			-0.09	0.45
PI-25_MI10	1.63	3.276E-01	2.02E-02	1.452E+05	7.090E-01	4.757E+04	7.15E-01	8.937E+04	24.91	0.40			0.03	0.45
PI-25_MI11	1.62	3.275E-01	2.10E-02	1.344E+05	6.070E-01	4.402E+04	6.08E-01	8.310E+04	24.70	0.42			-0.34	0.46
StH_mount2	1.62	3.294E-01	1.46E-02	2.767E+05	6.976E-01	9.111E+04	6.96E-01	1.713E+05	30.59	0.29	drift monitor			
PI-25_MI12	1.61	3.276E-01	2.66E-02	8.322E+04	3.447E-01	2.726E+04	3.53E-01	5.170E+04	25.01	0.53			-0.31	0.56
PI-25_MI15	1.61	3.277E-01	2.45E-02	9.846E+04	1.296E+00	3.227E+04	1.30E+00	6.133E+04	25.22	0.49			-0.22	0.52
PI-25_MI16	1.60	3.276E-01	1.66E-02	2.208E+05	7.701E-01	7.234E+04	7.75E-01	1.381E+05	25.18	0.33			-0.38	0.38
StH_mount2	1.60	3.296E-01	1.47E-02	2.744E+05	6.889E-01	9.043E+04	6.88E-01	1.718E+05	31.32	0.29	drift monitor			
PI-25_MI17	1.59	3.277E-01	2.10E-02	1.342E+05	6.107E-01	4.397E+04	6.17E-01	8.443E+04	25.39	0.42			-0.36	0.46
PI-25_MI20	1.59	3.279E-01	1.47E-02	2.721E+05	6.163E-01	8.921E+04	6.20E-01	1.716E+05	26.11	0.29			0.27	0.35
PI-25_MI19L	1.59	3.278E-01	2.09E-02	1.347E+05	6.475E-01	4.416E+04	6.52E-01	8.476E+04	25.64	0.42			-0.28	0.46
PI-25_MI19S	1.58	3.279E-01	2.11E-02	1.326E+05	6.141E-01	4.348E+04	6.20E-01	8.372E+04	25.92	0.42			-0.08	0.46
StH_mount2	1.58	3.299E-01	1.48E-02	2.701E+05	7.012E-01	8.910E+04	6.98E-01	1.713E+05	32.16	0.30	drift monitor			
StH_mount2	1.57	3.298E-01	1.48E-02	2.690E+05	6.788E-01	8.873E+04	6.78E-01	1.708E+05	32.03	0.30				
bg_mount2	1.57	3.396E-01	8.83E-02	7.039E+03	3.029E+00	2.394E+03	3.06E+00	4.486E+03	62.54	1.77	background			
StH_mount2	1.57	3.299E-01	1.49E-02	2.667E+05	6.903E-01	8.798E+04	6.89E-01	1.700E+05	32.16	0.30	drift monitor			
StH_mount2	1.56	3.299E-01	1.49E-02	2.655E+05	6.748E-01	8.760E+04	6.77E-01	1.702E+05	32.30	0.30	drift monitor			

Table S-4 Published values for key mixing reservoirs used to general fields in figures 1 and 2.

K/Cl	average	1σ	Min.	Max.	reference
Subducted marine sediments (SMS)					
UCC	63	65			Rudnick and Gao (2014)
UCC	41				Hans Wedepohl (1995)
Altered oceanic crust (AOC)					
Altered oceanic crust			0.3	2.0	Kendrick *et al.* (2013a)
Serpentinite					
Serpentinite	0.12	0.1	0.0	0.3	Kendrick *et al.* (2013b)
1000Br/Cl	**average**	**1σ**	**Min.**	**Max.**	**reference**
Subducted marine sediments (SMS)					
UCC	4.9	1.5	2	265	Han *et al.* (2023)
UCC	4.3				Rudnick and Gao (2014)
UCC	2.5				Hans Wedepohl (1995)
sedimentary rock	5.7	5.4			Kendrick *et al.* (2017)
Altered oceanic crust (AOC)					
Layer 3 AOC	1.9	1.2			Kendrick (2018)
Altered oceanic crust				<2.5	Kendrick *et al.* (2014)
Altered oceanic crust			0	3.5	Kendrick (2019)
Altered oceanic crust	1.7	1.6			Chavrit *et al.* (2016)
Serpentinite					
Serpentinite	3.3	0.9			Kendrick (2018)
Serpentinite	5.5	1.9	2.7	10.4	Kendrick *et al.* (2013b)
Serpentinite	4.7	7.2			Chavrit *et al.* (2016)
δ^{37}Cl	**average**	**1σ**	**Min.**	**Max.**	**reference**
Sediment and metasediment			-3.7	2.4	Bouvier *et al.* (2019)
Altered oceanic crust			-1.6	1.8	Bouvier *et al.* (2019)
Serpentinite			-2.7	2.4	Bouvier *et al.* (2019)
MORB			-1.04	0.37	Sharp *et al.* (2007)
^{87}Sr/^{86}Sr	**average**	**1σ**	**Min.**	**Max.**	**reference**
subducting sediments			0.7053	0.7080	Plank and Langmuir (1998)
Altered oceanic crust			0.7035	0.7075	Staudigel *et al.* (1995)
Serpentinite			0.7037	0.7095	Hattori and Guillot (2007)
DM			0.7020	0.7024	Zindler and Hart (1986)
^{3}He/^{4}He	**average**	**1σ**	**Min.**	**Max.**	**reference**
DM			11	7	Marty and Zimmermann (1999)

Table S-5 Partition coefficients used in source mantle calculation. Note, our bulk D_F and D_{Cl} differ from those in (JOACHIM *et al.*, 2015) (D_F = 0.08 and D_{Cl} = 0.03), the reason for this are unclear, however their bulk partition coefficients can be reproduced using D_F^{cpx}/D_F^{opx} = 5 and $D_{Cl}^{cpx}/D_{Cl}^{opx}$ = 1.5, rather than 1.5 and 5, respectively.

	X	D_F	D_{Cl}	D_{Br}	D_K
Olivine	0.62	0.028	0.029	0.029	0.0003
Orthopyroxene	0.24	0.066	0.027	0.027	0.0024
Clinopyroxene	0.12	0.098	0.136	0.136	0.0081
Bulk	0.98	0.045	0.041	0.041	0.0017

Table S-6 Composition of the N-PIP and E-PIP source calculated using the accumulated fractionation model based on samples PI-25 and CS-6, respectively. Compared to estimates for the composition of BSE, DM, lithospheric xenoliths and chondritic meteorites. Errors are 1 standard deviation.

	Method/Location	F (µg.g^{-1})	Cl (µg.g^{-1})	Br (µg.g^{-1})	1000Br/Cl
PIP source					
N-PIP source (PI-25, F=0.1)	Min-melt partitioning	19	9.2	0.104	11.3
E-PIP source (CS-6, F=0.25)	Min-melt partitioning	44	20	0.133	6.8
Depleted mantle					
Schilling *et al.* (1980)	Min-melt partitioning	65	7.3	0.02	2.74
Jambon *et al.* (1995)	Canonical ratio	-	~6	0.0075	1.25
Saal *et al.* (2002)	Canonical ratio	16 ± 3	1 ± 0.5	-	-
Salters and Stracke (2004)	Canonical ratio	11 ± 5	0.51 ± 0.09	-	-
Shimizu *et al.* (2016)	Canonical ratio	8.00	0.40	-	-
Joachim *et al.* (2015)	Min-melt partitioning	3-14	0.6-16	-	-
Kendrick *et al.* (2017)	Canonical ratio	12 ± 2	5 ± 2	0.013 ± 0.006	2.60
Guo and Korenaga (2021)	Log-log linear	54 ± 4.8	67 ± 26	0.049 ± 0.010	0.73
Bulk Silicate Earth					
McDonough and Sun (1995)	Canonical ratio	25	17	0.05	2.94
Palme and O'Neill (2014)	Mass balance + ratio	25 ± 10	30 ± 12	0.075 ± 0.038	2.50
Lyubetskaya and Korenaga (2007)	Canonical ratio	18 ±8	1.4 ± 0.5	0.0036 ± 0.0004	2.57
Kendrick *et al.* (2017)	Mass balance	17 ± 6	26 ± 8	0.076 ± 0.025	2.92
Guo and Korenaga (2021)	Log-log linear	57 ± 4.8	81 ± 24	0.091 ± 0.019	1.12
Intraplate lithospheric xenoliths					
Broadley *et al.* (2016)	West Antarctic				0.7-10
Kobayashi *et al.* (2019)	Eifel				0.5-4.5
Kobayashi *et al.* (2019)	Potrillo				0.1-4
Kobayashi *et al.* (2019)	San Carlos				3-7
CI Chondritic meteorites					
Wasson *et al.* (1997)	Compilation	64	680	3.6	5.29
Lodders and Fegley, 1998)	Compilation	60	717	3.34 ± 0.34	4.66
Palme and Zipfel (2022)	Orgueil	-	600 ± 68	2.68 ± 0.51	4.47
Palme and Zipfel (2022)	Ivuna	-	585	5.68	9.71
Palme and Zipfel (2022)	Alais	-	710	4.39	6.18
Palme and Zipfel (2022)	Tonk	-	510	9.01	17.7
CM Chondritic meteorites					
Wasson *et al.* (1997)	Compilation	38	160	2.6	16.3
Lodders and Fegley (1998)	Compilation	38	430	3	7.0
Reed and Allen (1966)	Mighei	-	350 ± 10	3.5 ± 1	10.0
Goles *et al.* (1967)	Mighei	-	430	3.9	9.1
Goles *et al.* (1967)	Mighei	-	510 ± 40	2.64 ± 0.03	5.2

Supplementary Figures

PI25-12 (mount 1)

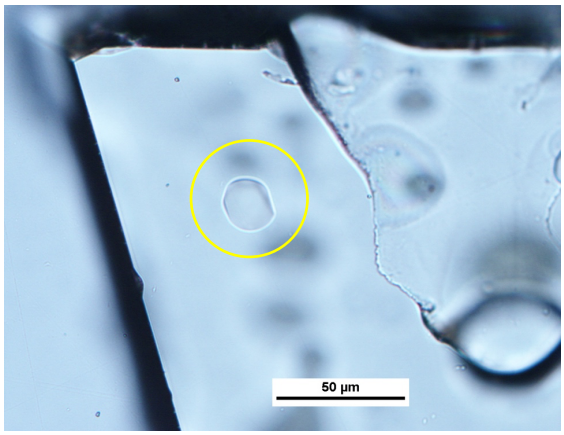

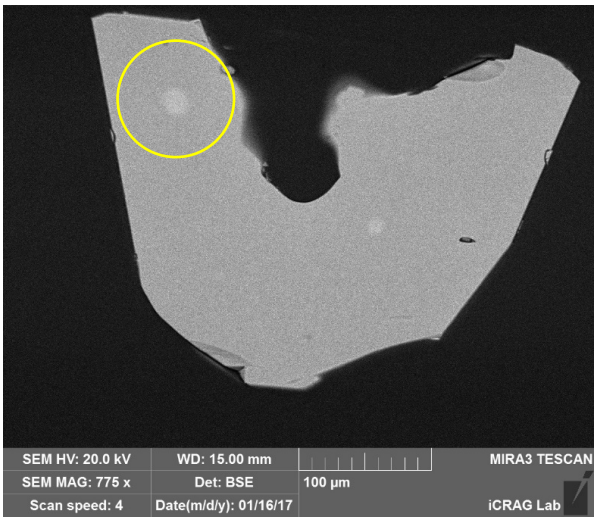

CS-5 3 (mount 3)

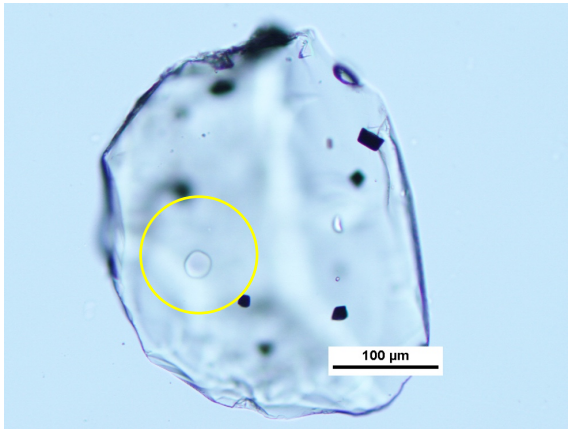

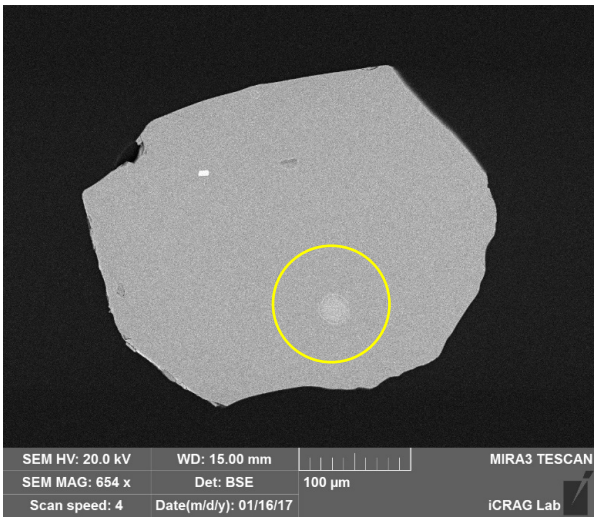

CS-6 1 (mount 3)

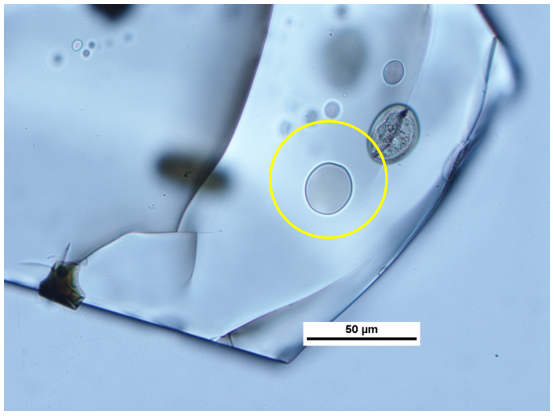

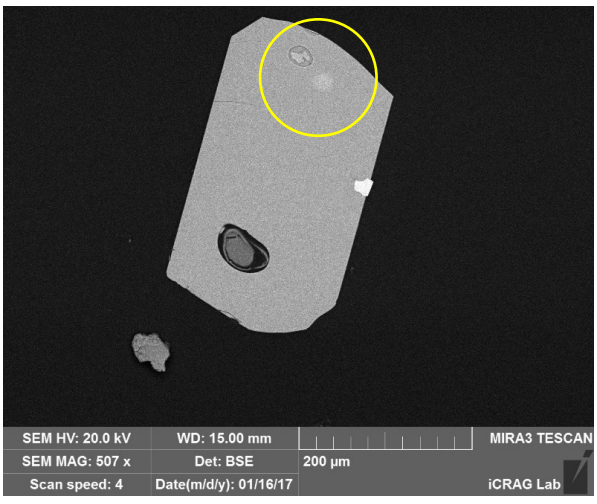

Figure S-1: Examples of the studied melt inclusions in transmitted light and Backscatter electron image.

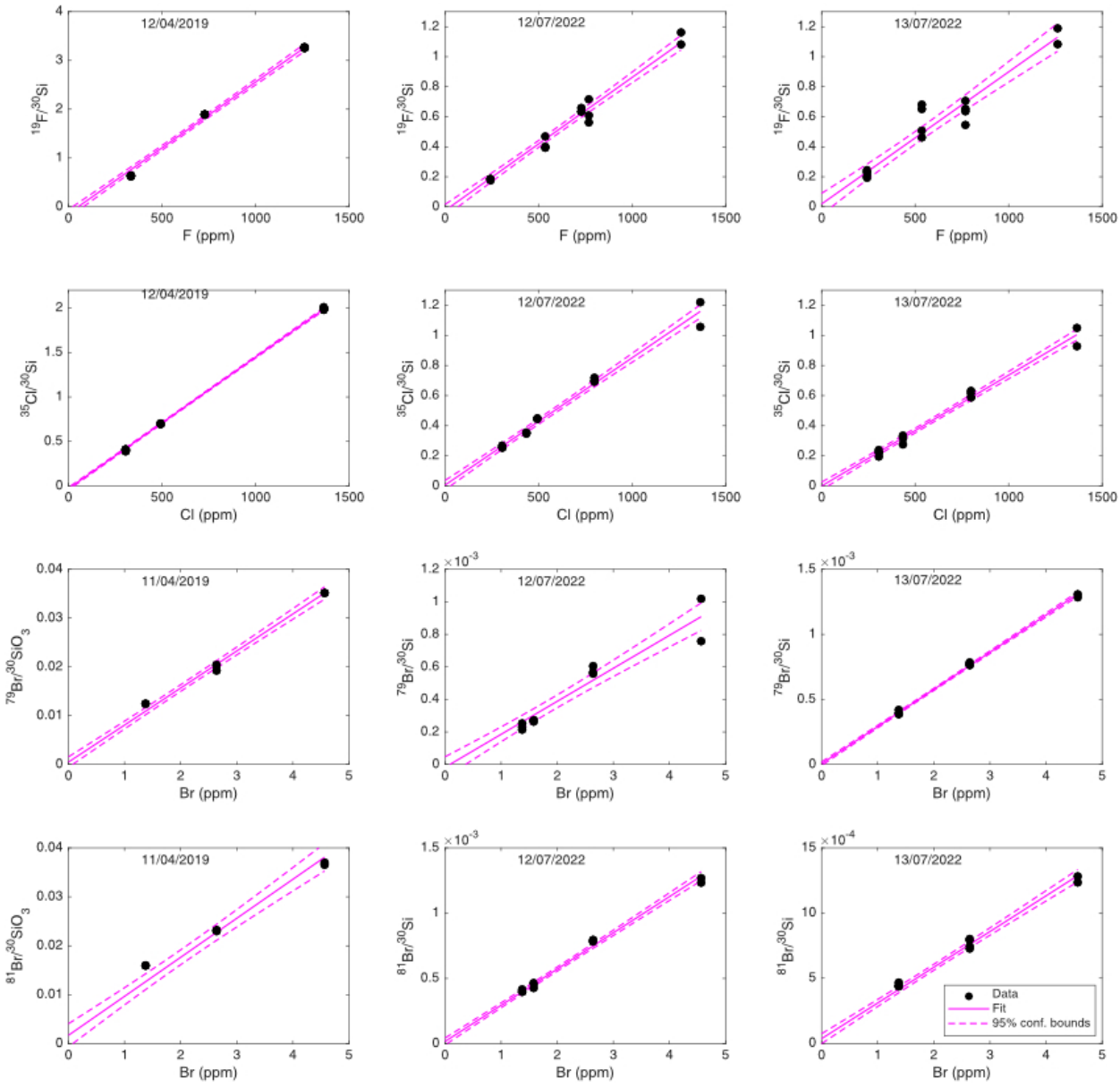

Figure S-2: Raw data for the calibration glass standards (in 2019: glasses VG-2, Macquarie 40428 and 47963; in 2022: glasses VG-2, Macquarie 25603, 40428, and 60701), the resulting calibration curves and their 95 % confidence intervals calculated by linear regression.

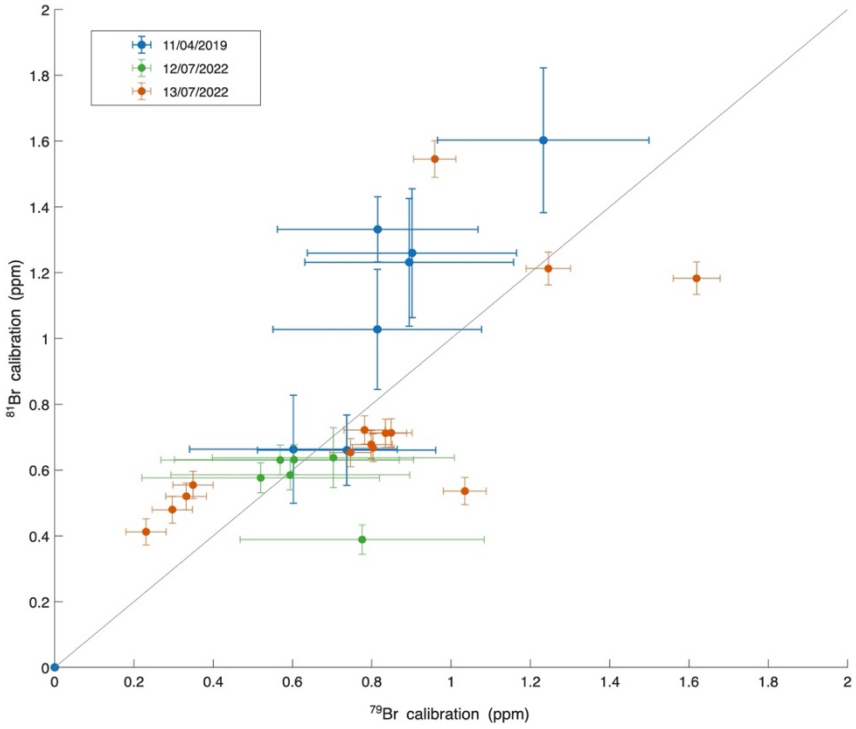

Figure S-3: Comparison between Br concentrations determined for unknowns (individual samples and quality control standards) using ^{81}Br and ^{79}Br, errors are propagated from the calibration curve.

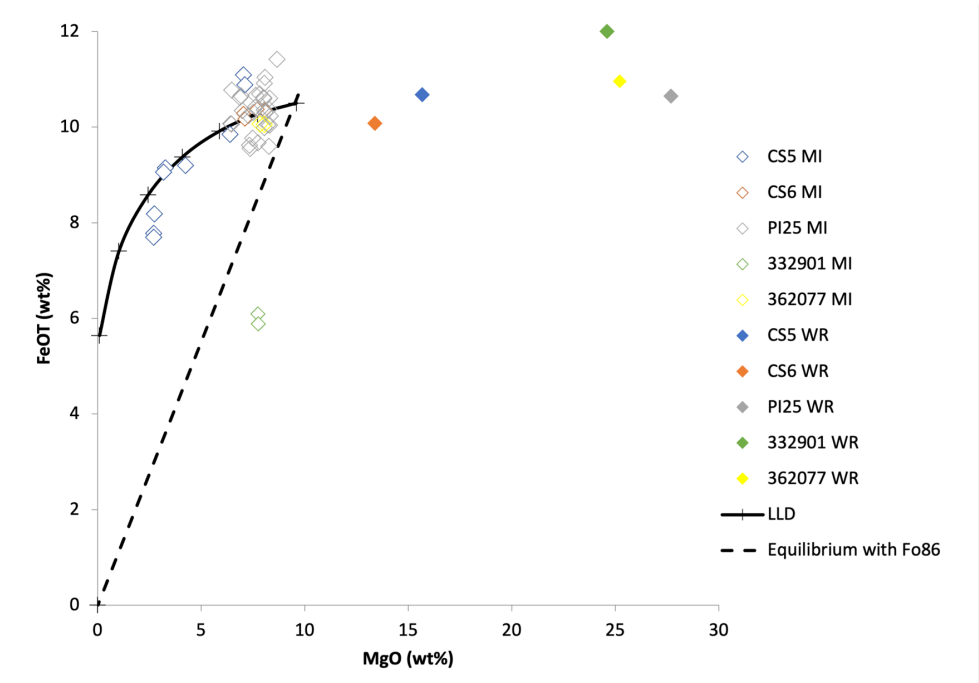

Figure S-4: Composition of PIP melt inclusions (this study) compared to the calculated liquid line of decent of melt DUR1 due to removal of olivine (+ markers show 5 % increments of olivine fractionation). Whole rock compositions are from Starkey *et al. (*2009). Also shown is the composition of melts in equilibrium with an olivine of a fixed composition of Fo_{86}.

Supplementary Information References

Bernstein, S., Hanghoj, K., Kelemen, P.B., Brooks, C.K. (2006) Ultra-depleted, shallow cratonic mantle beneath West Greenland: dunitic xenoliths from Ubekendt Ejland. *Contributions To Mineralogy and Petrology* 152, 335-347.

Bouvier, A.-S., Manzini, M., Rose-Koga, E.F., Nichols, A.R.L., Baumgartner, L.P. (2019) Tracing of Cl input into the sub-arc mantle through the combined analysis of B, O and Cl isotopes in melt inclusions. *Earth and Planetary Science Letters* 507, 30-39.

Broadley, M.W., Ballentine, C.J., Chavrit, D., Dallai, L., Burgess, R. (2016) Sedimentary halogens and noble gases within Western Antarctic xenoliths: Implications of extensive volatile recycling to the sub continental lithospheric mantle. *Geochimica Et Cosmochimica Acta* 176, 139-156.

Chavrit, D., Burgess, R., Sumino, H., Teagle, D.A.H., Droop, G., Shimizu, A., Ballentine, C.J. (2016) The contribution of hydrothermally altered ocean crust to the mantle halogen and noble gas cycles. *Geochimica Et Cosmochimica Acta* 183, 106-124.

Dalou, C., Koga, K.T., Le Voyer, M., Shimizu, N. (2014) Contrasting partition behavior of F and Cl during hydrous mantle melting: implications for Cl/F signature in arc magmas. *Progress in Earth and Planetary Science* 1, 26-26.

Dalou, C., Koga, K.T., Shimizu, N., Boulon, J., Devidal, J.L. (2012) Experimental determination of F and Cl partitioning between lherzolite and basaltic melt. *Contributions To Mineralogy and Petrology* 163, 591-609.

Dasgupta, R., Hirschmann, M.M., Smith, N.D. (2007) Partial Melting Experiments of Peridotite + CO2 at 3 GPa and Genesis of Alkalic Ocean Island Basalts. *Journal of Petrology* 48, 2093-2124.

Goles, G.G., Greenland, L.P., Jérome, D.Y. (1967) Abundances of chlorine, bromine and iodine in meteorites. *Geochimica Et Cosmochimica Acta* 31, 1771-1787.

Guo, M., Korenaga, J. (2021) A halogen budget of the bulk silicate Earth points to a history of early halogen degassing followed by net regassing. *Proceedings of the National Academy of Sciences* 118, e2116083118-e2116083118.

Han, P.-Y., Rudnick, R.L., He, T., Marks, M.A.W., Wang, S.-J., Gaschnig, R.M., Hu, Z.-C. (2023) Halogen (F, Cl, Br, and I) concentrations of the upper continental crust through time as recorded in ancient glacial diamictite composites. *Geochimica Et Cosmochimica Acta* 341, 28-45.

Hans Wedepohl, K. (1995) The composition of the continental crust. *Geochimica Et Cosmochimica Acta* 59, 1217-1232.

Hattori, K.H., Guillot, S. (2007) Geochemical character of serpentinites associated with high- to ultrahigh-pressure metamorphic rocks in the Alps, Cuba, and the Himalayas: Recycling of elements in subduction zones. *Geochemistry, Geophysics, Geosystems* 8.

Hauri, E.H., Gaetani, G.A., Green, T.H. (2006) Partitioning of water during melting of the Earth's upper mantle at H2O-undersaturated conditions. *Earth and Planetary Science Letters* 248, 715-734.

Herzberg, C., O'Hara, M.J. (2002) Plume-associated ultramafic magmas of phanerozoic age. *Journal of Petrology* 43, 1857-1883.

Jackson, M.G., Shirey, S.B. (2011) Re–Os isotope systematics in Samoan shield lavas and the use of Os-isotopes in olivine phenocrysts to determine primary magmatic compositions. *Earth and Planetary Science Letters* 312, 91-101.

Jambon, A., Déruelle, B., Dreibus, G., Pineau, F. (1995) Chlorine and bromine abundance in MORB: the contrasting behaviour of the Mid-Atlantic Ridge and East Pacific Rise and implications for chlorine geodynamic cycle. *Chemical Geology* 126, 101-117.

Jarosewich, E., Nelen, J.A., Norberg, J. (1980) Reference samples for electron microprobe analysis. *Geostandards Newsletter* 4, 43-47.

Joachim, B., Pawley, A., Lyon, I.C., Marquardt, K., Henkel, T., Clay, P.L., Ruzie, L., Burgess, R., Ballentine, C.J. (2015) Experimental partitioning of F and Cl between olivine, orthopyroxene and silicate melt at Earth's mantle conditions. *Chemical Geology* 416, 65-78.

Jochum, K.P., Stoll, B., Herwig, K., Willbold, M., Hofmann, A.W., Amini, M., Aarburg, S., Abouchami, W., Hellebrand, E., Mocek, B., Raczek, I., Stracke, A., Alard, O., Bouman, C.,

Becker, S., Dücking, M., BräTz, H., Klemd, R., de Bruin, D., Canil, D., Cornell, D., de Hoog, C.J., Dalpé, C., Danyushevsky, L., Eisenhauer, A., Gao, Y., Snow, J.E., Groschopf, N., Günther, D., Latkoczy, C., Guillong, M., Hauri, E.H., HöFer, H.E., Lahaye, Y., Horz, K., Jacob, D.E., Kasemann, S.A., Kent, A.J.R., Ludwig, T., Zack, T., Mason, P.R.D., Meixner, A., Rosner, M., Misawa, K., Nash, B.P., PfäNder, J., Premo, W.R., Sun, W.D., Tiepolo, M., Vannucci, R., Vennemann, T., Wayne, D., Woodhead, J.D. (2006) MPI-DING reference glasses for in situ microanalysis: New reference values for element concentrations and isotope ratios. *Geochemistry, Geophysics, Geosystems* 7, Q02008-Q02008.

John, T., Layne, G.D., Haase, K.M., Barnes, J.D. (2010) Chlorine isotope evidence for crustal recycling into the Earth's mantle. *Earth and Planetary Science Letters* 298, 175-182.

Kendrick, M. (2018) Halogens in Seawater, Marine Sediments and the Altered Oceanic Lithosphere. In: Harlov, D.E. and Aranovich, L. Eds.), *The Role of Halogens in Terrestrial and Extraterrestrial Geochemical Processes*. Springer, 591-648.

Kendrick, M.A. (2019) Halogens in altered ocean crust from the East Pacific Rise (ODP/IODP Hole 1256D). *Geochimica Et Cosmochimica Acta* 261, 93-112.

Kendrick, M.A., Arculus, R., Burnard, P., Honda, M. (2013a) Quantifying brine assimilation by submarine magmas: Examples from the Galapagos Spreading Centre and Lau Basin. *Geochimica Et Cosmochimica Acta* 123, 150-165.

Kendrick, M.A., Arculus, R.J., Danyushevsky, L.V., Kamenetsky, V.S., Woodhead, J.D., Honda, M. (2014) Subduction-related halogens (Cl, Br and I) and H2O in magmatic glasses from Southwest Pacific Backarc Basins. *Earth and Planetary Science Letters* 400, 165-176.

Kendrick, M.A., Hémond, C., Kamenetsky, V.S., Danyushevsky, L., Devey, C.W., Rodemann, T., Jackson, M.G., Perfit, M.R. (2017) Seawater cycled throughout Earth's mantle in partially serpentinized lithosphere. *Nature Geoscience* 10.

Kendrick, M.A., Honda, M., Pettke, T., Scambelluri, M., Phillips, D., Giuliani, A. (2013b) Subduction zone fluxes of halogens and noble gases in seafloor and forearc serpentinites. *Earth and Planetary Science Letters* 365, 86-96.

Kendrick, M.A., Kamenetsky, V.S., Phillips, D., Honda, M. (2012) Halogen systematics (Cl, Br, I) in Mid-Ocean Ridge Basalts: A Macquarie Island case study. *Geochimica Et Cosmochimica Acta* 81, 82-93.

Kobayashi, M., Sumino, H., Burgess, R., Nakai, S.i., Iizuka, T., Nagao, J., Kagi, H., Nakamura, M., Takahashi, E., Kogiso, T., Ballentine, C.J. (2019) Halogen Heterogeneity in the Lithosphere and Evolution of Mantle Halogen Abundances Inferred From Intraplate Mantle Xenoliths. *Geochemistry Geophysics Geosystems* 20, 952-973.

Larsen, L.M., Pedersen, A.K. (2000) Processes in High-Mg, High-T Magmas: Evidence from Olivine, Chromite and Glass in Palaeogene Picrites from West Greenland. *Journal of Petrology* 41, 1071-1098.

Le Voyer, M., Rose-Koga, E.F., Shimizu, N., Grove, T.L., Schiano, P. (2010) Two Contrasting H2O-rich Components in Primary Melt Inclusions from Mount Shasta. *Journal of Petrology* 51, 1571-1595.

Lodders, K., Fegley, B. (1998) The Solar System, *The Planetary Scientist's Companion*,

Lyubetskaya, T., Korenaga, J. (2007) Chemical composition of Earth's primitive mantle and its variance: 1. Method and results. *Journal of Geophysical Research: Solid Earth* 112.

Manzini, M., Bouvier, A.-S., Barnes, J.D., Bonifacie, M., Rose-Koga, E.F., Ulmer, P., Métrich, N., Bardoux, G., Williams, J., Layne, G.D., Straub, S., Baumgartner, L.P., John, T. (2017) SIMS chlorine isotope analyses in melt inclusions from arc settings. *Chemical Geology* 449, 112-122.

Marty, B., Zimmermann, L. (1999) Volatiles (He, C, N, Ar) in mid-ocean ridge basalts: assesment of shallow-level fractionation and characterization of source composition. *Geochimica Et Cosmochimica Acta* 63, 3619-3633.

McDonough, W.F. (1990) Constraints on the composition of the continental lithospheric mantle. *Earth and Planetary Science Letters* 101, 1-18.

McDonough, W.F., Sun, S.S. (1995) The composition of the Earth. *Chemical Geology* 120, 223-253.

Palme, H., O'Neill, H.S.C. (2014) Cosmochemical Estimates of Mantle Composition. *Treatise on Geochemistry* 2, 1-39.

Palme, H., Zipfel, J. (2022) The composition of CI chondrites and their contents of chlorine and bromine: Results from instrumental neutron activation analysis. *Meteoritics & Planetary Science* 57, 317-333.

Plank, T., Langmuir, C.H. (1998) The chemical composition of subducting sediment and its consequences for the crust and mantle. *Chemical Geology* 145, 325-394.

Reed, G.W., Allen, R.O. (1966) Halogens in chondrites. *Geochimica Et Cosmochimica Acta* 30, 779-800.

Roedder, P.L., Emslie, R.F. (1970) Olivine-Liquid Equilibrium. *Contributions To Mineralogy and Petrology* 29, 275-289.

Rose-Koga, E.F., Bouvier, A.S., Gaetani, G.A., Wallace, P.J., Allison, C.M., Andrys, J.A., Angeles de la Torre, C.A., Barth, A., Bodnar, R.J., Bracco Gartner, A.J.J., Butters, D., Castillejo, A., Chilson-Parks, B., Choudhary, B.R., Cluzel, N., Cole, M., Cottrell, E., Daly, A., Danyushevsky, L.V., DeVitre, C.L., Drignon, M.J., France, L., Gaborieau, M., Garcia, M.O., Gatti, E., Genske, F.S., Hartley, M.E., Hughes, E.C., Iveson, A.A., Johnson, E.R., Jones, M., Kagoshima, T., Katzir, Y., Kawaguchi, M., Kawamoto, T., Kelley, K.A., Koornneef, J.M., Kurz, M.D., Laubier, M., Layne, G.D., Lerner, A., Lin, K.Y., Liu, P.P., Lorenzo-Merino, A., Luciani, N., Magalhães, N., Marschall, H.R., Michael, P.J., Monteleone, B.D., Moore, L.R., Moussallam, Y., Muth, M., Myers, M.L., Narváez, D.F., Navon, O., Newcombe, M.E., Nichols, A.R.L., Nielsen, R.L., Pamukcu, A., Plank, T., Rasmussen, D.J., Roberge, J., Schiavi, F., Schwartz, D., Shimizu, K., Shimizu, N., Thomas, J.B., Thompson, G.T., Tucker, J.M., Ustunisik, G., Waelkens, C., Zhang, Y., Zhou, T. (2021) Silicate melt inclusions in the new millennium: A review of recommended practices for preparation, analysis, and data presentation. *Chemical Geology* 570, 120145.

Rose-Koga, E.F., Koga, K.T., Devidal, J.-L., Shimizu, N., Le Voyer, M., Dalou, C., Döbeli, M. (2020) In-situ measurements of magmatic volatile elements, F, S, and Cl, by electron microprobe, secondary ion mass spectrometry, and heavy ion elastic recoil detection analysis. *American Mineralogist* 105, 616-626.

Rudnick, R.L., Gao, S. (2014) Composition of the Continental Crust. *Treatise on Geochemistry* 4, 1-51.

Saal, A.E., Hauri, E.H., Langmuir, C.H., Perfit, M.R. (2002) Vapour undersaturation in primitive mid-ocean-ridge basalt and the volatile content of Earth's upper mantle. *Nature* 419, 451-455.

Salters, V.J.M., Stracke, A. (2004) Composition of the depleted mantle. *Geochemistry, Geophysics, Geosystems* 5.

Schiano, P. (2003) Primitive mantle magmas recorded as silicate melt inclusions in igneous minerals. *Earth-Science Reviews* 63, 121-144.

Schilling, J.g., Bergeron, M.B., Evans, R., Smith, J.V., Bailey, D.K., Tarney, J., Dunham, K.C. (1980) Halogens in the mantle beneath the North Atlantic. *Philosophical Transactions of the Royal Society of London. Series A, Mathematical and Physical Sciences* 297, 147-178.

Sharp, Z.D., Barnes, J.D., Brearley, a.J., Chaussidon, M., Fischer, T.P., Kamenetsky, V.S. (2007) Chlorine isotope homogeneity of the mantle, crust and carbonaceous chondrites. *Nature* 446, 1062-1065.

Shimizu, K., Saal, A.E., Myers, C.E., Nagle, A.N., Hauri, E.H., Forsyth, D.W., Kamenetsky, V.S., Niu, Y. (2016) Two-component mantle melting-mixing model for the generation of mid-ocean ridge basalts: Implications for the volatile content of the Pacific upper mantle. *Geochimica Et Cosmochimica Acta* 176, 44-80.

Sobolev, A., Dmitriev, L., Barsukov, V., Nevsorov, V., Slutskii, A. (1980) The formation conditions of high magnesium olivines from the monomineral fraction of Luna-24 regolith. *Proc. 11th Lunar Sci. Conf.* 11, 105-116.

Sobolev, A.V. (1996) Melt Incusions in Minerals as a source of principlepetrological information. *Petrology* 4, 209–220-209–220.

Starkey, N.A., Fitton, J.G., Stuart, F.M., Larsen, L.M. (2012) Melt inclusions in olivines from early Iceland plume picrites support high 3He/ 4He in both enriched and depleted mantle. *Chemical Geology* 306-307, 54-62.

Starkey, N.A., Stuart, F.M., Ellam, R.M., Fitton, J.G., Basu, S., Larsen, L.M. (2009) Helium isotopes in early Iceland plume picrites: Constraints on the composition of high 3He/4He mantle. *Earth and Planetary Science Letters* 277, 91-100.

Staudigel, H., Davies, G.R., Hart, S.R., Marchant, K.M., Smith, B.M. (1995) Large scale isotopic Sr, Nd and O isotopic anatomy of altered oceanic crust: DSDP/ODP sites417/418. *Earth and Planetary Science Letters* 130, 169-185.

Stephan, T., Jessberger, E.K., Klöck, W., Rulle, H., Zehnpfenning, J. (1994) TOF-SIMS analysis of interplanetary dust. *Earth and Planetary Science Letters* 128, 453-467.

Straub, S.M., Layne, G.D. (2003) The systematics of chlorine, fluorine, and water in Izu arc front volcanic rocks: Implications for volatile recycling in subduction zones. *Geochimica Et Cosmochimica Acta* 67, 4179-4203.

Wasson, J.T., Kallemeyn, G.W., Runcorn, S.K., Turner, G., Woolfson, M.M. (1997) Compositions of chondrites. *Philosophical Transactions of the Royal Society of London. Series A, Mathematical and Physical Sciences* 325, 535-544.

Zindler, A., Hart, S.R. (1986) Chemical Geodynamics. *Annual Reviews of Earth and Planetary sciences* 14, 493-571.